P-1022

v2.9
7 Nov. 2011

Revised Proposal: Intensity-Frontier Antiproton Physics with The Antiproton Annihilation Spectrometer (TAPAS*) at Fermilab

Giorgio Apollinari,[4] David M. Asner,[23] Wander Baldini,[5] Larry Bartoszek,[1] Daniel R. Broemmelsiek,[4] Charles N. Brown,[4] Alak Chakravorty,[24] Paul Colas,[2] Paul Derwent,[4] Alexey Drutskoy,[12] Michael Fortner,[20] Ioannis Giomataris,[2] Anjan Giri,[11] Keith Gollwitzer,[4] H. Richard Gustafson,[18] Alan Hahn,[4] Timothy Holmstrom,[16] Gerald P. Jackson,[7] Tord Johansson,[25] David E. Johnson,[4] Porter W. Johnson,[10] Daniel M. Kaplan,[10,*] Penelope Kasper,[4] ByeongRok Ko,[13] Kwong Lau,[9] Jonathan Lewis,[4] Mario Macri,[6] Mauro Marinelli,[6] Michael Merkin,[19] Sandip Pakvasa,[8] Vaia Papadimitriou,[4] HyangKyu Park,[14] Todd K. Pedlar,[17] Thomas J. Phillips,[3] Olga Piskunova,[15] Jerome Rosen,[21] Giulio Stancari,[4] Michelle Stancari,[4] Ray Stefanski,[4] Yagmur Torun,[10] James T. Volk,[4] Mitchell Wayne,[22] Steven Werkema,[4] William Wester,[4] Christopher G. White,[10] Herman B. White,[4] G. P. Yeh[4]

[1] *Bartoszek Engineering, Aurora, IL 60506, USA*
[2] *CEA Saclay, Gif-sur-Yvette, France*
[3] *Duke University, Durham, North Carolina 27708, USA*
[4] *Fermilab, Batavia, Illinois 60510, USA*
[5] *INFN, Sezione di Ferrara, Ferrara, Italy*
[6] *INFN, Sezione di Genoa, Genoa, Italy*
[7] *Hbar Technologies, LLC, West Chicago, Illinois 60185, USA*
[8] *University of Hawaii, Honolulu, Hawaii 96822, USA*
[9] *University of Houston, Houston, TX 77004, USA*
[10] *Illinois Institute of Technology, Chicago, Illinois 60616, USA*
[11] *Indian Institute of Technology, Hyderabad, India*
[12] *Institute for Theoretical and Experimental Physics, RU-117259 Moscow, Russia*
[13] *Korea University, Seoul, 136-701, Korea*
[14] *KyungPook National University, DaeGu, Korea*
[15] *Lebedev Physical Institute, RU-117924 Moscow, Russia*
[16] *Longwood University, Farmville, Virginia 23909, USA*
[17] *Luther College, Decorah, Iowa 52101, USA*
[18] *University of Michigan, Ann Arbor, Michigan 48109, USA*
[19] *Moscow State University, Moscow, Russia*
[20] *Northern Illinois University, DeKalb, Illinois 60115, USA*
[21] *Northwestern University, Evanston, Illinois 60208, USA*
[22] *Notre Dame University, Notre Dame, Indiana 46556, USA*
[23] *Pacific Northwest National Laboratory, Richland, Washington 99352, USA*
[24] *St. Xavier University, Chicago, Illinois 60655, USA*
[25] *Uppsala University, SE-751 05 Uppsala, Sweden*

*Spokesperson. E-mail address: kaplan@iit.edu

Summary

The Fermilab Antiproton Source is the world's most intense source of antimatter. With the Tevatron program now behind us, this unique facility can help make the case for Fermilab's continued accelerator operations. The Antiproton Source can be used for unique, dedicated antimatter studies, including medium-energy $\overline{p}$-annihilation experiments.

We propose to assemble a powerful, yet cost-effective, solenoidal magnetic spectrometer for antiproton-annihilation events, and to use it at the Fermilab Antiproton Accumulator to measure the charm production cross section, study rare hyperon decays, search for hyperon *CP* asymmetry, precisely measure the properties of several charmonium and nearby states, and make the first measurements of the Drell–Yan continuum in medium-energy antiproton annihilation. Should the charm production cross section be as large as some have proposed, we will also be able to measure D^0–$\overline{D}^0$ mixing with high precision and discover (or sensitively limit) charm *CP* violation. The observation of charm or hyperon *CP* violation would be evidence for physics beyond the Standard Model, with possible implications for the origin of the baryon asymmetry of the universe — the question of what happened to all the antimatter that must have been produced in the Big Bang.

The experiment will be carried out by an international collaboration and will require some four years of running time. As possibly the sole hadron experiment in progress at Fermilab during that time, it will play an important role in maintaining a broad particle physics program at Fermilab and in the U.S. It will thus help us to continue attracting creative and capable young people into science and technology, and introducing them to the important technologies of accelerators, detectors, and data acquisition and analysis — key roles in society that accelerator-based particle physics has historically played.

Contents

List of Figures

List of Tables

1 Introduction

We propose to assemble a simple, cost-effective, yet powerful magnetic spectrometer at the AP-50 experimental area of the Fermi National Accelerator Laboratory Antiproton Source, by integrating, and strategically augmenting, existing equipment from previous experiments. This will capitalize on Fermilab's very substantial investment in the Antiproton Source, by far the world's best facility for producing antiprotons. The TAPAS apparatus will allow uniquely sensitive investigations of

- hyperons,
- charmonium and nearby states,
- antiproton-induced Drell–Yan lepton pairs, and
- charm mesons.

We will use it to study and search for rare decays and symmetry-violating effects with world-leading sensitivities, and to make unique measurements of valence quarks in nucleons and nuclei at high x and low Q^2. Some of these measurements will be made for the first time, and others will improve on existing measurements by an order of magnitude or more.

This program of measurements, which could be completed by about 2018, may well constitute the only hadron physics carried out at Fermilab for many years prior to Project X turn-on. As such, it will substantially broaden the Lab's physics program and multiply the number of available thesis topics severalfold. It will thus help in attracting talented U.S. physics students into our field, and provide them with the valuable skills and experience that medium-scale accelerator-based experiments traditionally have done.

Table 1 compares the parameters of current and future antiproton sources. The highest-energy and highest-intensity antiproton source is at Fermilab. Even while stacking only 15% of the time (so as to allow fixed-target collisions the rest of the time), it can support a luminosity of $2 \times 10^{32}\,\mathrm{cm}^{-2}\mathrm{s}^{-1}$ on an internal target. The CERN Antiproton Decelerator (AD)

Table 1: Antiproton energies and intensities at existing and future facilities.

Facility	$\overline{p}$ Kinetic Energy (GeV)	Stacking: Rate (10^{10}/hr)	Stacking: Duty Factor	Operation: Hours /yr	Operation: $\overline{p}$/yr (10^{13})
CERN AD	0.005 0.047	–	–	3800	0.4
Fermilab Accumulator:					
current operation	8	>25	90%	5550	>150
proposed here	≈ 3.5–8	20	15%	5550	17
FAIR ($\gtrsim 2018$*)	1–14	3.5	15%*	2780*	1.5

*The lower number of operating hours at FAIR compared with that at other facilities arises from the collection ring being shared between the antiproton and radioactive-beam programs. Due to the modular staging of the FAIR facility, stacking of antiprotons will initially be done in the experiment ring, leading to the small duty factor shown here. FAIR's stacking ring is planned for installation several years after initial operation.

provides low-energy antiproton beams at a tiny fraction of the intensity available at Fermilab. Germany's billion-Euro plan for the Facility for Antiproton and Ion Research (FAIR) at Darmstadt includes construction — only just beginning — of 30 and 90 GeV rapid-cycling synchrotrons, and of low- and medium-energy antiproton and ion storage rings [1]. Antiproton operation at FAIR is not anticipated before 2018. The Fermilab Antiproton Source has previously served medium-energy antiproton fixed-target experiments, including the charmonium experiments E760 and E835. With the completion of the Tevatron program, it is once again potentially available for dedicated antiproton experiments. For the selected topics we propose, it is the world's most sensitive facility, and will remain so for many years.

It is worth noting in Table 1 that an additional order of magnitude in intensity becomes available if the Antiproton Source can stack full-time. This offers the possibility of a luminosity upgrade (to $\sim 10^{33}\,\mathrm{cm}^{-2}\mathrm{s}^{-1}$) by adding a small third ring to the complex. The rate capability of the detector would need to be upgraded accordingly. One would then have a sensitivity for small cross sections and for high-statistics measurements with which FAIR would be unable to compete for the foreseeable future. The detector capabilities at $\mathcal{L} \sim 10^{32}\,\mathrm{cm}^{-2}\mathrm{s}^{-1}$ could also be upgraded, by (for example) building a new calorimeter, with photodetectors that are insensitive to magnetic fields, and a new spectrometer solenoid to go around it.

We believe these potential upgrades are worth considering, but that they should be designed based on measured cross sections for signals and backgrounds, rather than on the models and simulations that are currently available, which are likely to be unreliable due to the paucity of data on which they are based. Thus a relatively quick experiment based largely on available equipment is the logical next step in pursuing antiproton physics at Fermilab, provided such an experiment has enough capability to be compelling on its own. We argue in the following that it does.

2 TAPAS Physics Overview

In the flavor problem, nature has handed us a supremely challenging puzzle. Forty years since the Standard Model's founding, our failure to discern what deeper theory underlies it bespeaks the difficulty of the challenge. The clues being few, we can ill afford to ignore any area where new ones might lie. The progress of technology now enables unprecedented sensitivities to rare effects, giving access to new-physics signatures previously thought too difficult to pursue.

Several important issues can be studied in a medium-energy antiproton-beam fixed-target experiment. These include the possible contributions of new physics to hyperon decay and charm mixing and decay, and the mechanism(s) underlying the mysterious X, Y, and Z states in the charmonium region [2]. Without knowing the nature of the new physics we seek, it is difficult to rank these by impact and importance. But should new physics be *discovered* in any one of them, it would immediately become the most interesting particle-physics topic of the day. Despite much effort on B and K mixing and CP violation (CPV), evidence for physics beyond the Standard Model in those sectors has proved elusive [3].[1] We should therefore look elsewhere as well. The key questions — whether new physics contributes appreciably to hyperon decay, charm decay, or charm mixing — hinge on the degree to which these phenomena violate CP symmetry [5].

[1] The evidence for anomalous CP violation in B_s mixing observed by the DØ collaboration [4], if confirmed, may indicate that new physics does indeed contribute to CP asymmetries at detectable levels.

New sources of *CP* violation are expected by many. The baryon asymmetry of the universe can in principle be understood in terms of *CP* violation [6], but the CKM contribution to CPV is too small by many orders of magnitude [7], suggesting that additional contributions from new physics were at play in the early universe. Proposed Standard Model extensions (e.g., non-minimal SUSY [8], multi-Higgs models [9], left–right-symmetric models [10, 11], and the SME of Kostelecký *et al.* [12]) abound in possible new, *CP*-violating phases, which could account for the baryon asymmetry and could show up in sensitive heavy-quark experiments. These issues have motivated substantial, world-wide efforts seeking to discover physics beyond the Standard Model in neutral-meson mixing and CPV. We are proposing to take the next step in sensitivity in hyperons and charm. At the same time we will have the opportunity to shed light on an intriguing, current mystery — the nature of the $X(3872)$ and its cousins — and perform unique and valuable measurements of parton distribution functions via the Drell–Yan process.

As recently emphasized at PANIC11 by G. Perez [13], both the K and B sectors appear consistent with minimal flavor violation, suggesting that the non-SM CPV that baryogenesis requires must reside elsewhere. He therefore stressed the importance of the search for new physics in charm, where SM CPV is strongly suppressed. In an alternate view, it is now fashionable to hope that the "action" will be in the neutrino sector — baryogenesis via leptogenesis — a prospect whose thorough testing will take decades and giga-dollars. The importance of the issue impels us toward a thorough, near-term investigation in charm and hyperons — the more so since the opportunity to do so is so cost-effective, and so synergistic with the current situations of Fermilab and of U.S. HEP. We stress that in a healthy research enterprise, experiments at widely differing funding levels ought not to compete with one another. For example, TAPAS will not materially affect the construction or running schedule of LBNE.

The lack of signals to date at LHC for supersymmetry or other new physics serves to remind us that virtual effects accessible in intensity-frontier experiments cover a much wider mass range than does the LHC. Perez [13] and many previous authors [14, 15, 16] have shown that D^0 mixing and charm CPV and rare decays (for example) already provide some of the strongest bounds on new-physics mass scales and couplings, with masses in the 10^3 TeV region or higher if unit coupling strengths are assumed. We must not "put all our eggs in the LHC basket." To the contrary, we must exploit these intensity-frontier opportunities to learn about virtual effects due to new physics at scales that are inaccessible via direct production.

2.1 Hyperons

While CPV is by now well studied in the K^0 and B-meson sectors, CPV in hyperon decay has yet to be established. Its relative suppression in the Standard Model creates an observational window in which new physics could play a dominant role. Such is also the case for rare hyperon decays. Two potentially interesting hyperon signals may already have been glimpsed in the Fermilab HyperCP experiment, albeit with low statistical significance: evidence for *CP* violation observed via the $A_{\Xi\Lambda}$ asymmetry parameter in ${}^{(}\overline{\Xi}{}^{)}{}^{\mp}$ decay [17], and for flavor-changing neutral currents in Σ^+ decay [18]. While a dedicated experiment to follow up each of these $< 3\sigma$ effects would be hard to justify, the opportunity for substantial increases in hyperon statistics using the same apparatus that can make the other measurements described here is highly appealing. Some R&D will be required to assess the feasibility of improving on the $\Xi^-/\overline{\Xi}^+$ sensitivity achieved by HyperCP. In any case, we will

be able to study Σ^+ and Ω^- decays and search for $\Omega^-/\overline{\Omega}^+$ *CP* violation with unprecedented sensitivities,[2] and world-leading ${}^{(}\overline{\Xi}{}^{)}{}^{\mp}$ studies may also be possible. These hyperon measurements offer a window into new physics different from, and complementary to, those of K, B, and D mesons. As detailed below, we aim to achieve sensitivity to both the $A_{\Xi\Lambda}$ and Δ_Ω *CP* asymmetries at the $\approx 1 \times 10^{-4}$ level. This is three times better than the HyperCP $A_{\Xi\Lambda}$ result. There is no previous measurement of Δ_Ω.

It might be argued that such signals will be difficult to interpret theoretically, even if they are (say) an order of magnitude larger than expected in the Standard Model. However, in our experience, such physics is invariably led, and driven, by experiment. A significant observation of an apparent new-physics CPV signal will be a major breakthrough, and will stimulate the ingenuity of theorists in ways that current phenomenological speculation cannot. Furthermore, by pushing sensitivities for more than just a single hyperon *CP* asymmetry, we will create the opportunity to observe multiple interesting signals, whose pattern could tell us more than would a single observation.

2.2 Charmonium and X(3872)

The $X(3872)$ has been observed by several groups (see Table 2) and is a well established state [19]. Despite its proximity in mass to various charmonium levels, it does not appear to be a charmonium state itself [2]. As we will see, $\overline{p}p$ annihilation has the potential to make uniquely incisive measurements of its properties and thereby reveal its true nature.

Table 2: Experimental observations of $X(3872)$.

Expt.	Year	Mode	Events	Ref.
Belle	2003	$\pi^+\pi^- J/\psi$	35.7 ± 6.8	[20]
BABAR	2004	$\pi^+\pi^- J/\psi$	25.4 ± 8.7	[21]
CDF	2004	$\pi^+\pi^- J/\psi$	730 ± 90	[22]
DØ	2004	$\pi^+\pi^- J/\psi$	522 ± 100	[23]
Belle	2004	$\omega(\pi^+\pi^-\pi^0) J/\psi$	10.6 ± 3.6	[24]
Belle	2005	$\gamma J/\psi$	13.6 ± 4.4	[25]
Belle	2006	$D^0\overline{D}{}^0\pi^0$	23.4 ± 5.6	[26]
BABAR	2008	$\gamma\psi$, $\gamma\psi'$	23.0 ± 6.4, 25.4 ± 7.3	[27]
BABAR	2008	$D^0\overline{D}{}^0\pi^0$	33 ± 7	[28]

By scanning the Antiproton Accumulator beam energy across the resonance, Fermilab experiments E760 and E835 made the world's most precise measurements of charmonium masses and widths [29, 30]. This technique can be used to measure the $X(3872)$ mass, width, and lineshape with a precision unobtainable by any other means. At present [19], the upper limit on the $X(3872)$ width is 2.3 MeV. With $\sim$1000 events, we aim to measure its mass and its width with to ~ 100 keV.

The other key advantage of $\overline{p}p$ annihilation is its ability to directly produce charmonium states of all quantum numbers, in contrast to e^+e^- machines which produce primarily 1^{--} states and the few states that couple directly to them, or (with lower statistics) states accessible in B decay or 2γ production. In addition to studying the $X(3872)$, now that the

[2]For convenience, inclusion of charge-conjugate decays is hereinafter implied where not otherwise stated.

masses of the η_c' and h_c are reasonably well determined [19], detailed scans dedicated to the spectroscopy of both states are possible, and should be performed.

The various X, Y, and Z states appear to pose intriguing and important questions [31]. Some have been interpreted as charmonium states, others as coupled-channel effects, tetraquarks, or meson-antimeson molecules. There may be a new spectroscopy coming into view — an exciting prospect. So far they have been observed only in e^+e^- annihilation or in B decays. The opportunity to bring a new methodology — $\overline{p}p$ formation — to bear on the problem could be extremely valuable.

2.3 Antiproton Drell–Yan Studies

Measurements of Drell–Yan lepton-pair production have played a key role in determining sea-quark and gluon distributions in the nucleon. Global structure-function fits to deep-inelastic lepton-scattering and Drell–Yan data form the foundation for our understanding of important Tevatron and LHC cross sections. This involves extrapolation from high-x measurements obtained at low Q^2 to the low-x and high-Q^2 collisions (mainly of gluons) at the LHC that can produce (for example) Higgs bosons or supersymmetric particles. However, data at high x and low Q^2 are very sparse. Antiproton collisions at the Antiproton Source offer the opportunity for unprecedented studies of Drell–Yan production at high x and low Q^2.

Moreover, the global structure-function fits suffer from poor χ^2 values, reflecting tension among the various data sets. In these fits, valence-quark distributions are determined predominantly from deep-inelastic scattering data, while sea distributions depend predominantly on Drell–Yan data. These two distinct categories of experimental data have differing biases, nuclear effects, and systematic uncertainties, which appear not to be fully understood. In contrast, antiproton-beam Drell–Yan data directly measure valence distributions, offering the opportunity to determine both valence and sea distributions for the first time from just one type of measurement: Drell–Yan.

2.4 Charm-Meson Mixing, CP Violation, and Rare Decays

As pointed out by many authors (see for example [3, 14, 15, 16, 32, 33]), charm presents an excellent venue in which to search for new physics. Not only is it the only up-type quark for which mixing is observable, but Standard Model backgrounds to new physics are suppressed in charm: the CKM factors are small, and the most massive quark participating in loop diagrams is the b. There are thus many potential signatures in charm (such as CPV in D^0–$\overline{D}^0$ mixing) that would be direct indications of new physics. Furthermore, compared to beauty, charm has both a large hadroproduction cross section and large branching ratios to decay modes of interest.

In the past, the largest charm samples have been obtained in high-energy hadroproduction experiments (e.g., Fermilab E791 and, now, CDF) and at the B factories. We argue that over the next several years, a medium-energy charm experiment at the Fermilab Antiproton Source might be the world's most sensitive:

1) hadroproduction has an enormous charm-production advantage over e^+e^- colliders: charm hadroproduction cross sections are typically $\sim\mu$b, vs. 1 nb for e^+e^-;

   and

2) the low charged-particle multiplicity in medium-energy $\overline{p}$ annihilation offers a substantial signal-to-background advantage over hadroproduction at high energy.

Of course, luminosity favors e^+e^- (by factors of 10 to 10^2), and until now, backgrounds have as well. Moreover, *high*-energy hadroproduction has the advantage of longer decay distances. But the higher charged-particle multiplicity ($\langle n_{ch}\rangle \gtrsim 10$) [19] in high-energy interactions is responsible for the dominant background to charm in high-energy experiments — combinatorics — whose suppression has required tight vertex cuts. The much lower charged-particle multiplicity ($\langle n_{ch}\rangle \approx 3$) [19] in $\overline{p}$ collisions near open-charm threshold should lead to charm samples with cleanliness comparable to that at the B factories, with the application of only modest cuts, and hence, high efficiency. As we will see, antiproton annihilation at the Fermilab Accumulator may thus enable the reconstruction of clean charm-meson decay samples a factor of ten or more larger than those of the B factories.

The competition to medium-energy $\overline{p}$ collisions is LHC*b* (discussed further below), which may have significant systematic biases, due e.g. to trigger effects, production and detection asymmetries, and large rates of $b \to c$ decays, and a possible "super-B factory"; when such a facility will be in full-luminosity operation is at present uncertain. The immediate question for us is whether Fermilab should seek to continue to compete in this area. We believe the answer is a clear yes.

3 Experimental Approach

We have proposed [34] to assemble an "upgraded E835" apparatus (Fig. 1), including a magnetic spectrometer, with precision vertexing and particle-identification capabilities. Since the E835 apparatus did not include a magnet, various cross sections needed to assess experiment performance and reach remain unmeasured; however, they can be estimated with some degree of confidence. If these cross sections are of the expected magnitudes, it should be possible with this apparatus to make the world's best measurements of hyperon rare decays and CPV, charm mixing and CPV, as well as of the other states mentioned above. At a minimum, besides precision charmonium measurements, the experiment will measure several cross sections for the first time. Because much of the equipment and infrastructure needed for this experiment are already available, needing only to be integrated rather than built from scratch, we are offered a remarkable and unusual opportunity to do valuable physics quickly and at modest cost.

The E760/835 barrel calorimeter, in storage at Fermilab, can easily be reinstalled in the AP-50 pit. A spectrometer solenoid that fits inside the calorimeter is available at KEK. Charged-particle tracking can be performed with scintillating fibers, taking advantage of the very capable scintillating-fiber readout system from the Fermilab DØ experiment [35] which, with the end of the Tevatron program, now becomes available. Precision ($\delta t < 10\,\mathrm{ps}$ r.m.s.), cost-effective time-of-flight (TOF) counters under development [36] are likely to be available by the time they are needed for this experiment. High-bandwidth triggering and data-acquisition systems will be needed, and again can exploit hardware available from DØ and CDF. The estimated assembly and installation costs, summarized in Table 3, total less than $10M. We estimate the time from start of funding to initial shakedown at about 2 years. Apparatus details are presented in Sec. 5, and the budget and schedule are detailed in Sec. 6.

We assume $\overline{p}p$ or $\overline{p}N$ luminosity of $2 \times 10^{32}\,\mathrm{cm}^{-2}\mathrm{s}^{-1}$, one order of magnitude beyond that of E835, which can be accomplished by use of a denser internal target than the E835

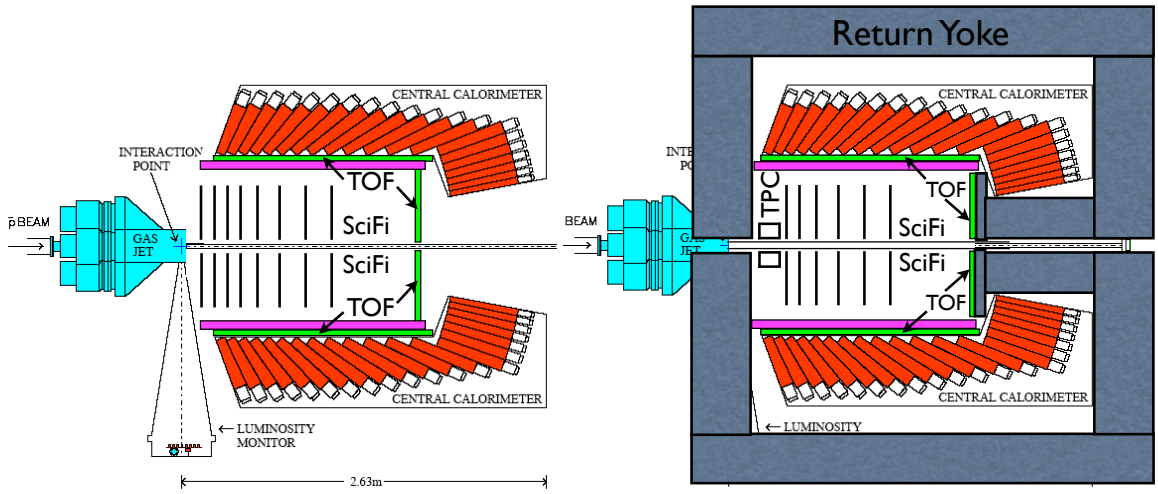

Figure 1: Sketch of (left) "upgraded E835" apparatus as simulated: a 1 T solenoid surrounds fine-pitch scintillating-fiber detectors, and is surrounded by precision TOF counters, all within the existing E760/835 Central Calorimeter (return yoke not shown); (right) current apparatus baseline, including small Time Projection Chamber and return yoke needed for proper functioning of calorimeter phototubes.

Table 3: Construction and Installation Budget Summary; see Sec. 6.2 for details.

Item	Cost (k$)	Contingency (k$)
Targets	430	160
Luminosity monitor	60	20
Scintillating-fiber tracking system	1,820	610
Time-of-Flight system	500*	500
Triggering	1,390	460
Data acquisition system	490	153
Infrastructure	1,350	550
TOTALS	6,040	2,450

*Detailed TOF cost estimates based on the University of Chicago "Large-Area Picosecond Photo-Detectors" project are not yet available. This is a preliminary estimate from H. Frisch, for which we assume 100% contingency.

hydrogen cluster-jet [37]. This could be a cryogenic, frozen-hydrogen target (already under development, as discussed in Sec. 5.2) or a thin metal wire or pellet; these would be operated in the halo of the antiproton beam.[3]

[3]A denser cluster-jet target may also be a possibility and is under development by the $\overline{\text{P}}$ANDA collaboration [38].

4 Measurement Program

Of the suite of measurements we propose, some can be performed simultaneously, while others must be carried out sequentially due to their particular beam-energy requirements. For example, precision measurements of the $X(3872)$ require scanning of the beam energy across the resonance in small steps, while the Ω *CP*-violation study requires running somewhat above the 3345 MeV threshold for $\overline{p}p \to \overline{\Omega}^+\Omega^-$, and Drell–Yan and charm-meson studies are likely to be optimized by running at the highest available Accumulator beam kinetic energy, 8 GeV. We are thus proposing a measurement *program* which will take approximately 4 years; the schedule is discussed further in Sec. 6. It should also be noted that the $X(3872)$ running *requires* a hydrogen target, and the charm running may benefit from one but could also use a metal target, while the hyperon running could be done with a hydrogen or a metal target, and Drell–Yan data should be taken with both hydrogen and nuclear targets.

We next discuss in greater detail each of the major proposed measurements.

4.1 Hyperon CP Violation and Rare Decays

Hyperon *CP* asymmetries probe parity-*conserving* currents, hence they can potentially provide information about new physics that is complementary to that from the B and K systems.[4] Hyperon CPV measurements have yet to reach Standard Model (CKM) sensitivity levels, but possible new-physics contributions can stand out, and be detected, against the small CKM background. The world's largest hyperon samples are from the Fermilab HyperCP Experiment [39], including 2.1×10^9 reconstructed Ξ^- and 0.5×10^9 $\overline{\Xi}^+$ decays, and 10^{10} produced Σ^+. The main HyperCP goal was to substantially advance sensitivity to the ${}^{(}\overline{\Xi}{}^{)}{}^{\mp} \to {}^{(}\overline{\Lambda}{}^{)}\pi^{\mp}$ decay-angle *CP* asymmetry, $A \equiv (\alpha+\overline{\alpha})/(\alpha-\overline{\alpha})$ [40], where α ($\overline{\alpha}$) is the hyperon (antihyperon) longitudinal parity-violation parameter [41]. In this it succeeded, extending sensitivities by some two orders of magnitude over previous results.

HyperCP observed unexpected possible signals at the $>2\sigma$ level for new physics in the rare hyperon decay $\Sigma^+ \to p\mu^+\mu^-$ [18] (Fig. 2) as well as in the *CP* asymmetry $A_{\Xi\Lambda} \approx A_\Xi + A_\Lambda = [-6.0 \pm 2.1\,(\text{stat}) \pm 2.0\,(\text{syst})] \times 10^{-4}$ [17]. It also set the world's first limit on CPV in Ω^- decay: $A_{\Omega\Lambda} = [-0.4 \pm 9.1\,(\text{stat}) \pm 8.5\,(\text{syst})] \times 10^{-2}$ [42]. Since the $\overline{p}p \to \overline{\Omega}^+\Omega^-$ threshold lies in the same mass region as charmonium, the proposed experiment can further test these observations using $\Omega^- \to \Xi^-\mu^+\mu^-$ decays and potential ${}^{(}\overline{\Omega}{}^{)}{}^{\mp}$ CPV, signaled e.g. by possible small Ω–$\overline{\Omega}$ decay-rate differences in ${}^{(}\overline{\Lambda}{}^{)}K^{\mp}$ or ${}^{(}\overline{\Xi}{}^{)}{}^0\pi^{\mp}$ final states [43]. It may also be possible to run just above the $\overline{p}p \to \overline{\Xi}^+\Xi^-$ threshold and improve on the statistics and systematics of the HyperCP $A_{\Xi\Lambda}$ measurement. Note that while the HyperCP evidence is suggestive of the range of possible new-physics effects in hyperon decay, high-sensitivity hyperon studies are well motivated more generally, irrespective of the HyperCP signals.

While *CPT* symmetry requires the lifetimes of particle and antiparticle to be identical, partial-rate asymmetries violate only *CP*. For most hyperon decays, partial-rate asymmetries are expected to be undetectably small. However, this need not be the case for Ω^- decays to ΛK^- and $\Xi^0\pi^-$, for which the particle/antiparticle partial-rate asymmetries could be as large as 2×10^{-5} in the Standard Model and one to two orders of magnitude larger if non-SM contributions are appreciable [43]. These are quantities for which there are no

[4] While ϵ_K is also sensitive to parity-conserving currents, it is consistent with arising entirely from the SM, hence offers little direct information about new physics.

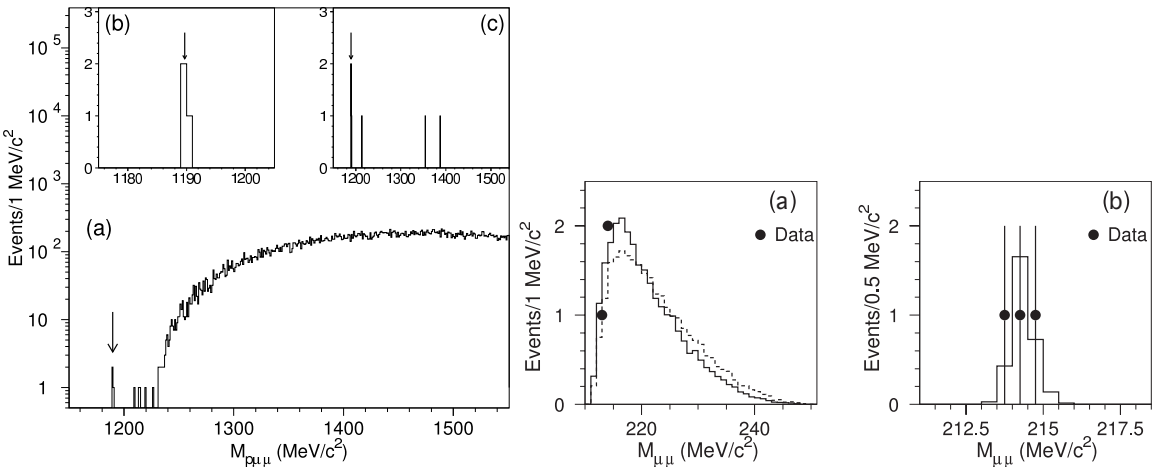

Figure 2: (Left) Mass spectrum for 3-track final states consistent with being single-vertex $p\mu^+\mu^-$ events in HyperCP positive-beam data sample: (a) wide mass range (semilog scale); (b) narrow range around Σ^+ mass; (c) after application of additional cuts as described in Ref. [18]. (Arrows indicate mass of Σ^+.) (Right) Dimuon mass spectrum of the three HyperCP $\Sigma^+ \to p\mu^+\mu^-$ candidate events compared with Monte Carlo spectrum assuming (a) SM virtual-photon form factor (solid) or isotropic decay (dashed), or (b) decay via a narrow resonance X^0. The mass distribution is consistent with a new narrow resonance, with 2.4σ statistical significance.

previous measurements. The quantities to be measured are

$$\Delta_{\Lambda K} \equiv \frac{\Gamma(\Omega^- \to \Lambda K^-) - \Gamma(\overline{\Omega}^+ \to \overline{\Lambda} K^+)}{\Gamma(\Omega^- \to \Lambda K^-) + \Gamma(\overline{\Omega}^+ \to \overline{\Lambda} K^+)} \,, \; \Delta_{\Xi\pi} \equiv \frac{\Gamma(\Omega^- \to \Xi^0\pi^-) - \Gamma(\overline{\Omega}^+ \to \overline{\Xi}^0\pi^+)}{\Gamma(\Omega^- \to \Xi^0\pi^-) + \Gamma(\overline{\Omega}^+ \to \overline{\Xi}^0\pi^+)} \tag{1}$$

$$\approx \frac{1}{2\Gamma}(\Gamma - \overline{\Gamma}) \tag{2}$$

$$\approx 0.5\,(1 - N/\overline{N})\,, \tag{3}$$

where in the last step we have assumed equal numbers (N) of Ω and ($\overline{N}$) of $\overline{\Omega}$ events, as would be the case in the experiment proposed here. As a benchmark, sensitivity at the 10^{-4} level thus requires $\mathcal{O}(10^7)$ reconstructed events. Measuring such a small branching-ratio difference reliably will require the clean, exclusive event sample produced less than a π^0 mass above threshold, or $4.94 < p_{\overline{p}} < 5.44\,\mathrm{GeV}/c$. As detailed below, running at this momentum, we expect to obtain 10^8 exclusive $\overline{p}p \to \overline{\Omega}^+\Omega^-$ events. We have begun simulation studies of the limiting systematics in such measurements, with promising results, indicating that 10^{-4} sensitivity is likely achievable.

Besides partial-rate differences, other possible new-physics signals in Ω decay include decay-angle asymmetries [42], T-odd asymmetries in e.g. $\Omega^- \to \Xi^-\pi^+\pi^-$ [44], and confirmation of the HyperCP $\Sigma^+ \to p\mu^+\mu^-$ signal in $\Omega^- \to \Xi^-\mu^+\mu^-$, where, due to the greater Q value, the branching ratio is expected to be of $\mathcal{O}(10^{-6})$ if the X^0 possibly observed in HyperCP is real [45].[5] The experiment we propose will extend sensitivities in all such sig-

[5]Such a particle, if confirmed, could be evidence for nonminimal supersymmetry [46] or other new physics [47, 48].

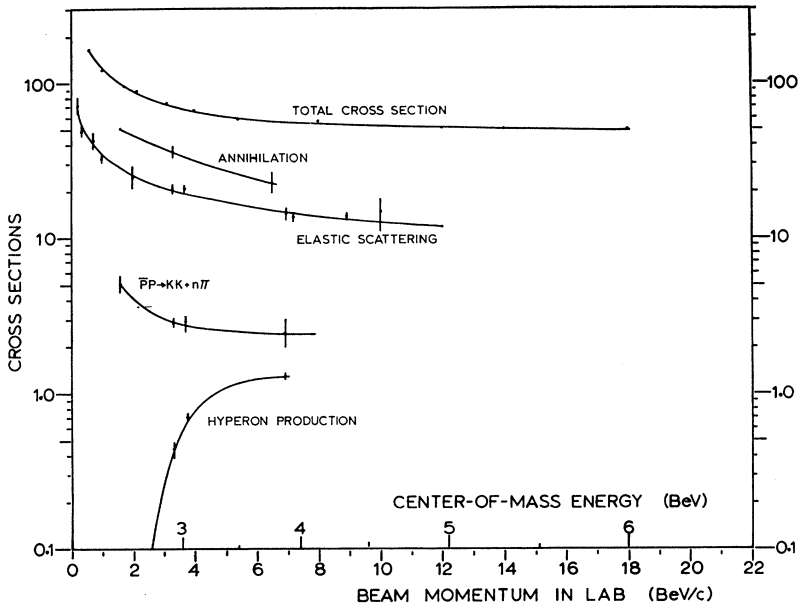

Figure 3: Cross sections (in mb) for various $\overline{p}p$ processes vs. momentum and $\sqrt{s}$ (from [53]).

natures. (The recent negative evidence for $X^0 \to \mu^+\mu^-$ in K [49] and B decays [50] does not entirely rule out the possibility that the "HyperCP particle" is real — although it does significantly restrict its parameter space — since the B^0 and K^0 decay modes in question probe couplings of the X^0 different from those in hyperon decay [51].)

4.1.1 Hyperon sensitivity estimates

There have been numerous measurements of hyperon production by low-energy antiprotons. Johansson *et al.* [52] report cross sections measured by PS185 at LEAR, but the maximum LEAR $\overline{p}$ momentum ($2\,\mathrm{GeV}/c$) was insufficient to produce Ξ's or Ω's. Chien *et al.* [53] report measurements of a variety of hyperon final states, performed with the BNL 80-inch liquid-hydrogen bubble chamber, in a $6.935\,\mathrm{GeV}/c$ electrostatically separated antiproton beam at the AGS; Baltay *et al.* [54] summarize data taken at lower momenta. In 80,000 pictures Chien *et al.* observed some 1,868 hyperon or antihyperon events, corresponding to a total hyperon-production cross section of $1.310 \pm 0.105\,\mathrm{mb}$ [53]. The corresponding cross section measured at $3.7\,\mathrm{GeV}/c$ was $720 \pm 30\,\mu\mathrm{b}$, and $438 \pm 52\,\mu\mathrm{b}$ at $3.25\,\mathrm{GeV}/c$ [54] (see Fig. 3). The inclusive hyperon-production cross section at $5.4\,\mathrm{GeV}/c$ is thus about 1 mb. At $\mathcal{L} = 2 \times 10^{32}\,\mathrm{cm}^{-2}\mathrm{s}^{-1}$ this amounts to some 2×10^5 hyperon events produced per second, or 4×10^{12} per year.

To estimate the exclusive $\overline{p}p \to \overline{\Omega}\Omega$ cross section requires some extrapolation, since it has yet to be measured (moreover, even for $\overline{p}p \to \overline{\Xi}^+\Xi^-$ only a few events have been seen). A rule of thumb is that each strange quark costs between one and two orders of magnitude in cross section, reflecting the effect of the strange-quark mass on the hadronization process. This is borne out by e.g. HyperCP, in which 2.1×10^9 $\Xi^- \to \Lambda\pi^-$and 1.5×10^7 $\Omega^- \to \Lambda K^-$ decays were reconstructed [39]; given the $160\,\mathrm{GeV}/c$ hyperon momentum and 6.3 m distance from HyperCP target to decay pipe, this corresponds to ≈ 30 Ξ^-'s per Ω^- produced at the target. A similar ratio is observed in HERA-B [55]. In exclusive $\overline{p}p \to$ hyperon-antihyperon production there could be additional effects, since as one proceeds from Λ to Ξ to Ω fewer

Table 4: Measured and estimated $\overline{p}p \rightarrow$ hyperon-antihyperon cross sections just above threshold.

Reaction	$\overline{p}$ momentum	Cross section	Ref.
$\overline{p}p \rightarrow \Lambda\overline{\Lambda}$	1.642	$\approx 65\,\mu$b	[52]
$\overline{p}p \rightarrow \Xi^-\overline{\Xi}^+$	3.0	$\approx 2\,\mu$b*	[54, 56]
$\overline{p}p \rightarrow \Omega^-\overline{\Omega}^+$	5.4	$\approx 60\,$nb	–

*While the cross section at 3.0 GeV/c $\overline{p}$ momentum has not been measured, that at 3.5 GeV/c has been and is shown here.

and fewer valence quarks are in common between the initial and final states. Nevertheless, the cross section for $\overline{\Xi}^+\Xi^-$ somewhat above threshold ($p_{\overline{p}} \approx 3.5\,\mathrm{GeV}/c$) is $\approx 2\,\mu$b [54, 56, 57], or about 1/30 of the corresponding cross section for $\overline{\Lambda}\Lambda$. Thus the $\approx 65\,\mu$b cross section measured for $\overline{p}p \rightarrow \overline{\Lambda}\Lambda$ at $p_{\overline{p}} = 1.642\,\mathrm{GeV}/c$ at LEAR [52] implies $\sigma(\overline{p}p \rightarrow \overline{\Omega}\Omega) \approx 60\,$nb at $5.4\,\mathrm{GeV}/c$ (Table 4).

The forgoing extrapolation implies $\approx 2 \times 10^8$ $\overline{\Omega}\Omega$ events produced per year. For detector acceptance times efficiency of 50% and given the various branching ratios, an estimated 2.1×10^7 decays each in $\Omega^- \rightarrow \Xi^0\pi^-$ and $\overline{\Omega}^+ \rightarrow \overline{\Xi}^0\pi^+$ are observed, and 6.1×10^7 each in $\Omega^- \rightarrow \Lambda K^-$ and $\overline{\Omega}^+ \rightarrow \overline{\Lambda}K^+$, giving the following statistical sensitivities for partial-rate asymmetries:

$$\delta\Delta_{\Xi\pi} \approx \frac{0.5}{\sqrt{N_{\Xi\pi}}} \approx 1.1 \times 10^{-4}\,, \tag{4}$$

$$\delta\Delta_{\Lambda K} \approx \frac{0.5}{\sqrt{N_{\Lambda K}}} \approx 6.4 \times 10^{-5}\,. \tag{5}$$

At these sensitivities, if the *CP* asymmetry in $\Xi^- \rightarrow \Lambda\pi^-$ is as large as suggested by HyperCP, one might expect to see signals in one or both of these Ω decay modes. Note that in $\overline{p}p \rightarrow \overline{\Omega}\Omega$, no valence quarks are in common between the initial and final states, thus the Ω and $\overline{\Omega}$ should have similar kinematics, thereby minimizing systematic uncertainties. (Further in the future — but beyond the scope of this Proposal — an additional, dedicated $\overline{p}$ storage ring could decelerate antiprotons to the $\Lambda\overline{\Lambda}$, $\Sigma^+\overline{\Sigma}^-$, and $\Xi^-\overline{\Xi}^+$ thresholds, where an experiment at 10^{33} luminosity might amass the clean, $>10^{10}$-event samples needed to definitively confirm or refute the HyperCP evidence [17] for *CP* asymmetry in the $\Xi^- \rightarrow \Lambda\pi^-$ decay sequence; alternatively, efficient deceleration to the $\Xi^-\overline{\Xi}^+$ threshold region might be possible in the existing Accumulator, but its feasibility is yet to be established.[6] The feasibility of such a precise *CP*-asymmetry measurement has been argued in [57].)

In addition, the measured $\approx 1\,$mb cross section for associated production of inclusive hyperons [53] would mean $\sim 10^{12}$ Σ^+ events produced per year, which could directly confront the HyperCP evidence (at $\approx 2.4\sigma$ significance) for a possible new particle of mass $214.3\,\mathrm{MeV}/c^2$ in the three observed $\Sigma^+ \rightarrow p\mu^+\mu^-$ events (Fig. 2).

[6] Whether the the existing Accumulator suffices to amass the needed statistics at $\Xi^-\overline{\Xi}^+$ threshold depends on the efficiency of decelerating in the Accumulator to $\approx 3.0\,\mathrm{GeV}/c$, which in turn depends on how the lattice is manipulated as the beam crosses transition, or so as to avoid transition crossing altogether [59] — a complex set of questions, requiring R&D that can only be performed with dedicated use of the Antiproton Source.

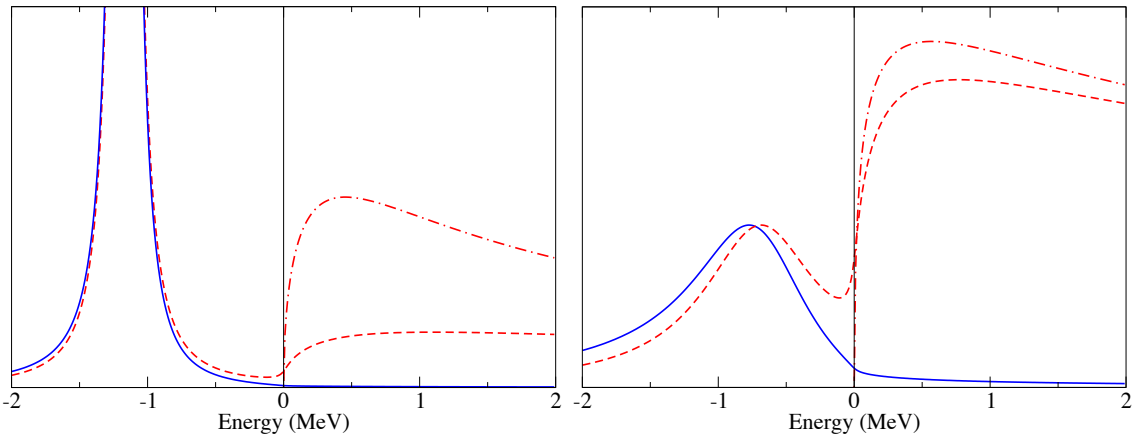

Figure 4: Examples of expected $X(3872)$ lineshapes in $J/\psi\pi^+\pi^-$ (solid-blue curve) and $D^0\overline{D}^0\pi^0$ (dashed-red) final states for various parameter choices in the molecular hypothesis (from [58]).

4.2 Precision Measurements in the Charmonium Region

Using the Fermilab Antiproton Source, experiments E760 and E835 made the world's most precise measurements of charmonium masses and widths [29, 30]. This precision ($< 100\,\mathrm{keV}$) was enabled by the small energy spread of the stochastically cooled antiproton beam and the absence of Fermi motion and negligible energy loss in the H_2 cluster-jet target. Although charmonium has by now been extensively studied, a number of questions remain, most notably the nature of the mysterious $X(3872)$ state [2] and improved measurement of h_c and η_c' parameters [31]. The width of the X may well be small compared to 1 MeV [58]. The unique precision of the $\overline{p}p$ energy-scan technique is ideally suited to making the precise mass, lineshape, and width measurements needed to test the intriguing hypothesis that the $X(3872)$ is a $D^{*0}\overline{D}^0$ molecule [60]. As shown in Fig. 4, in the molecular hypothesis, the lineshape of the $X(3872)$ will be distinctive and dependent on decay mode. For optimal $\sqrt{s}$ resolution, these measurements will require the use of a hydrogen target: either an improved version of the E835 gas jet or a windowless, frozen-hydrogen target [61] (see below).

The formation cross section of $X(3872)$ in $\overline{p}p$ annihilation has not been measured, but it has been estimated to be similar in magnitude to that of the χ_c states [62, 63]. In E760, the χ_{c1} and χ_{c2} were detected in $\overline{p}p \to \chi_c \to \gamma J/\psi$ (branching ratios of 36% and 20%, respectively [19]) with acceptance times efficiency of $44 \pm 2\%$, giving about 500 observed events each for an integrated luminosity of $1\,\mathrm{pb}^{-1}$ taken at each resonance; at the mass peak, 1 event was observed per nb^{-1} [64]. The lower limit $\mathcal{B}[X(3872) \to \pi^+\pi^- J/\psi] > 0.042$ at 90% C.L. [65] implies that in a day at the peak of the $X(3872)$ ($8\ \mathrm{pb}^{-1} \times$ [1000 events/pb^{-1}] $\times\, 0.04/0.36 \times$ acceptance-efficiency ratio of final states of $\approx 50\%$), about 500 events would be observed. Even if the formation cross section is an order of magnitude less than those of the χ_c states, the tens of events per day of running at the peak will be greater than the background observed by E835.[7] By way of comparison, Table 2 shows current sample sizes, which are likely to increase by not much more than an order of magnitude as the respective analyses are completed. (Although CDF and DØ could amass samples of order 10^4 $X(3872)$ decays, the large backgrounds in the CDF and DØ observations, reflected

[7] This $\overline{p}p \to X(3872)$ sensitivity will be competitive even with that of the SuperKEKB [66] upgrade.

in the uncertainties on the numbers of events listed in Table 2, limit their incisiveness.)

We have concentrated here on one decay mode of the $X(3872)$: $X(3872) \to \pi^+\pi^- J/\psi$. Large samples will of course also be obtained in other modes as well, increasing the statistics and allowing knowledge of $X(3872)$ branching ratios to be improved. Given the uncertainties in the cross section and branching ratios, the above may well be an under- or overestimate of the $\overline{p}p$ formation and observation rates, perhaps by as much as an order of magnitude. Nevertheless, it appears that a new experiment at the Antiproton Accumulator could obtain the world's largest clean samples of $X(3872)$, in perhaps as little as a month of running. In a few months of running, hundreds to thousands of observed events can be expected in all of the known decay modes, and many more, as-yet-unknown, modes should be seen as well. We will also have the opportunity to study the angular distributions of both the known and unknown modes. The high statistics, event cleanliness, and unique precision available in the $\overline{p}p$ formation technique could enable the world's smallest systematics. This experiment could thus provide a definitive test of the nature of the $X(3872)$. Although others of the X, Y, and Z particles are not as narrow as the $X(3872)$, their $\overline{p}p$ formation and observation in a variety of decay modes could nevertheless shed light on whether a new spectroscopy of meson-antimeson molecules, multiquark states, gluonic hybrids — or something else entirely — is being glimpsed.

4.3 Antiproton Drell–Yan

Figure 5 compares the NLO Drell–Yan lepton-pair production cross sections, computed using a next-to-leading order (NLO) CTEQ code [67], for 8 GeV (kinetic) pp and $\overline{p}p$ collisions. We see that the presence of valence antiquarks in the antiproton amplifies the Drell–Yan cross section by about a factor of 20 at $1.25\,\mathrm{GeV}/c^2$ mass in $\overline{p}p$ as compared to pp collisions. Moreover, the "amplification" factor increases with mass. The ability to measure this cross section depends on the sizes of the dominant backgrounds, which are expected to be lepton pairs from the independent semileptonic decays of charm-anticharm pairs, and pion pairs misidentified as lepton pairs. We have simulated each of these backgrounds based on plausible models and find them to be one to two orders of magnitude below the signal for masses in the range $2.0 < m < 3.0\,\mathrm{GeV}/c^2$ (beyond which the J/ψ should dominate the signal).

In the corresponding range of lepton momentum, electrons can be distinguished from pions more readily than can muons. We thus propose to use e^+e^- pairs to measure the Drell–Yan cross section. The particle identification criteria available include comparison of the calorimetric energy to the magnetically measured momentum (E/p), calorimeter transverse shower shape, time-of-flight (TOF) measurement, and ionization-rate (dE/dx) measurement in the TPC. E/p cuts alone typically provide π/e rejection of 10^{-3} per track. Combining this rejection with that from shower shape, dE/dx and TOF, we expect to suppress the random-pion-pair background by a factor of 10^{-10}. Furthermore, the main backgrounds will each be measured with high statistics, allowing a precision background subtraction to be performed.

Figure 6 shows the $\overline{p}p$ Drell–Yan cross section integrated over Feynman-x, and Fig. 7 compares it with the simulated background spectra. We have estimated the π/e-misidentification background by generating 8 GeV fixed-target $\overline{p}p$ events in Geant4 [68], forming all possible $\pi^+\pi^-$ pairs in each event, and scaling the resulting mass spectrum down by 10^{-10}. We have estimated the charm background by generating $D^*\overline{D}$ pairs and allowing them to decay semileptonically, assuming a $\overline{p}p \to D^*\overline{D}$ cross section of $3\,\mu$b. We see that while charm is the dominant background over most of the useful mass range, the

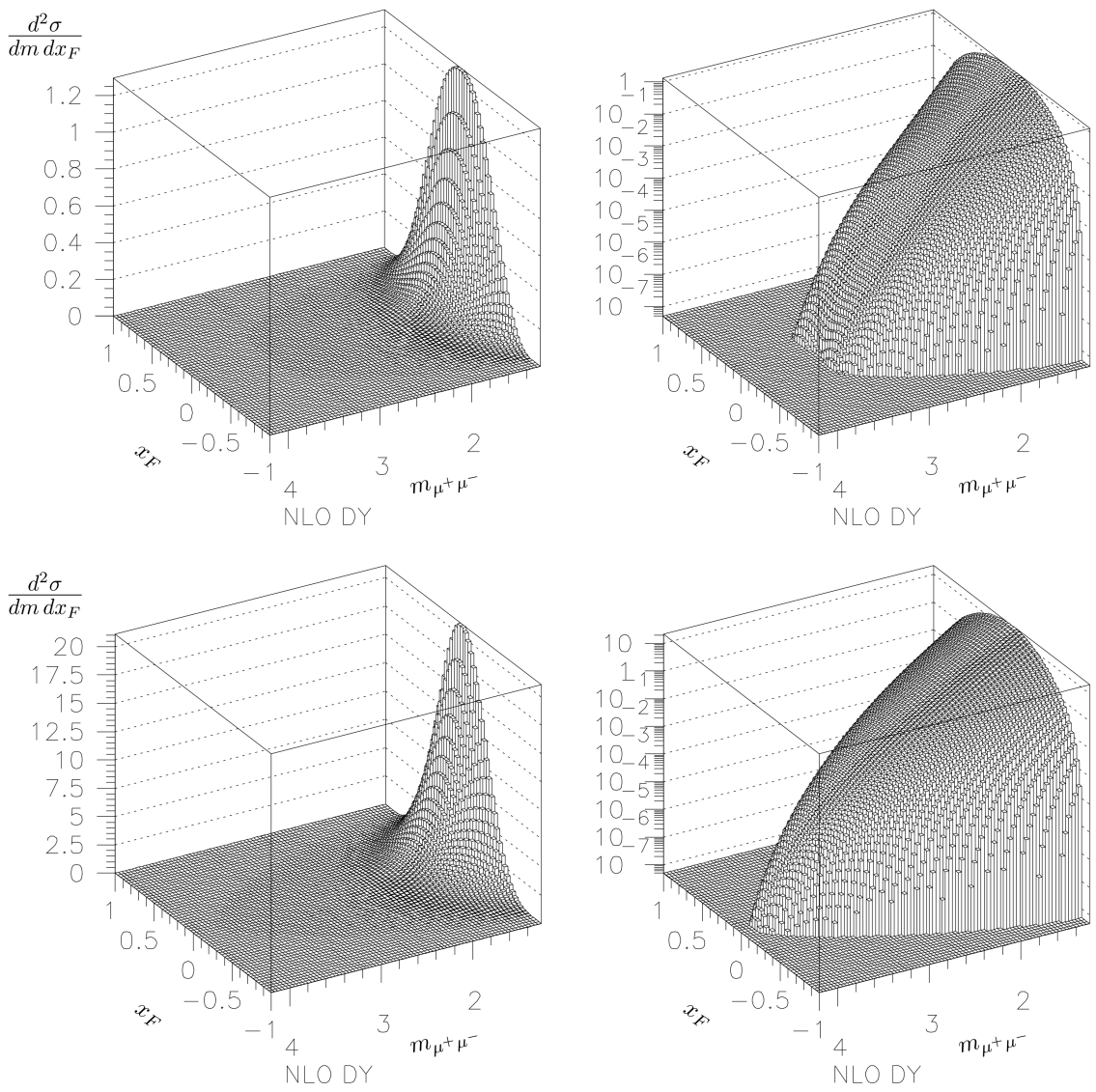

Figure 5: Doubly differential NLO Drell–Yan cross sections in (top) pp and (bottom) $\overline{p}p$ fixed-target collisions at 8 GeV p or $\overline{p}$ kinetic energy, as calculated by P. Reimer using CTEQ code [67]. Units of x and z axes are GeV/c^2 and nb/GeV, respectively.

Drell–Yan signal does appear large enough to be measured.

Studies of $\overline{p}p$-produced Drell–Yan dileptons at 8 GeV can also address the following outstanding physics issues:

1. The Lam–Tung relation [69], derived in the 1980s as a consequence of the spin-1/2 nature of the quarks, was found to be significantly violated in pion-induced Drell–Yan data [70, 71]. More recent Drell–Yan results from Fermilab E866 [72, 73] in pp and pd, and from CDF $\overline{p}p$ at large dilepton p_t and mass [74], showed that the violation is much less pronounced than in the pion data. The origin of the violation of the Lam–Tung relation is still poorly understood. Drell–Yan data from TAPAS, measured in a very different kinematic regime compared to previous results, could provide unique new information.

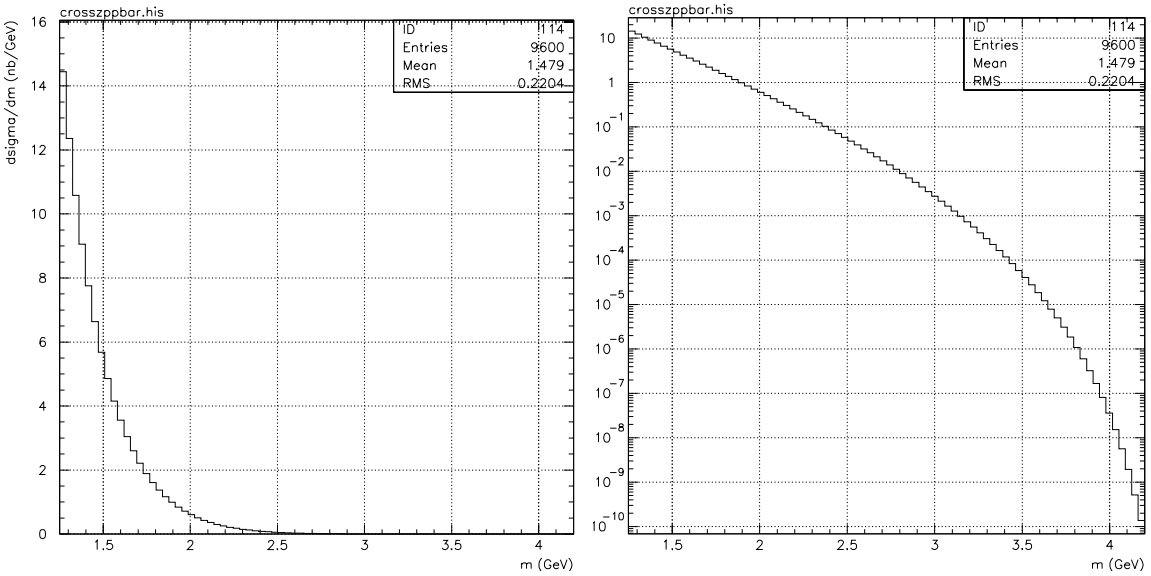

Figure 6: Mass spectrum of Drell–Yan $\ell^+\ell^-$ pairs in fixed-target $\overline{p}p$ collisions with 8 GeV $\overline{p}$ kinetic energy as calculated to NLO, on linear and semilogarithmic scales. (Based on calculation by Reimer [67].)

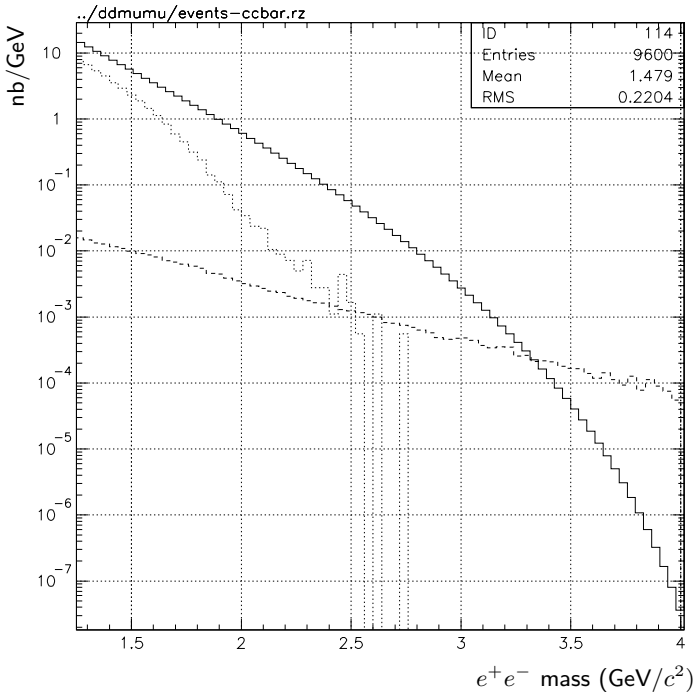

Figure 7: CTEQ NLO Drell–Yan signal (solid histogram) [67] with simulated $\pi^+\pi^-$-mis-ID (dashed) and $c\overline{c}$-double-semileptonic (dotted) backgrounds superimposed, assuming 10^{-5} background rejection per pion track. Additional rejection of the charm background may be possible using vertex information.

2. It has been pointed out [75] that measurement of the azimuthal angular distribution (the "$\cos 2\phi$" term) of the Drell–Yan process can be used to extract a novel transverse-momentum–dependent parton distribution function known as the Boer–Mulders function. The Boer–Mulders function corresponds to the correlation between the quark transverse spin and the quark transverse momentum in an unpolarized hadron. Pronounced $\cos 2\phi$ azimuthal angular dependence has been observed in pion-induced [70, 71], but not in proton-induced [72, 73], Drell–Yan production. This difference is interpreted as a consequence of the valence-like nature of the Boer–Mulders function probed using pion beams, since proton-induced Drell–Yan involves the sea-quark Boer–Mulders function. TAPAS could further test this since the valence-valence nature of $\overline{p}p$ collisions implies that the azimuthal $\cos 2\phi$ angular dependence should be large. These data could also provide additional input for extracting these novel Boer–Mulders functions.

3. There is considerable interest in accurate measurements of the Q^2 dependence of the Weinberg mixing angle using parity-violating reactions [76]. The NuTeV anomaly remains to be understood, and major new experiments have been proposed at the Jefferson Laboratory to measure parity violation in electron deep-inelastic scattering and in Møller scattering. TAPAS Drell–Yan data would provide a unique opportunity to study parity violation at the Q^2 scale of a few GeV^2. The interference of the virtual-photon and Z^0 exchange would show up as a forward-backward asymmetry in the Drell–Yan data [77]. A simulation study is currently underway to determine the feasibility of such a measurement and will be reported at the PAC meeting.

4. It has been predicted that the Drell–Yan cross sections could be significantly higher than indicated by the NLO calculation when "threshold resummation" is taken into account [78]. The kinematics of the TAPAS Drell–Yan events would be ideal for a stringent test of this prediction. This information is also crucial for future Drell–Yan experiments being planned at the FAIR antiproton and the J-PARC proton facilities where relatively low energy antiproton and proton beams will be utilized.

4.4 Charm Mixing, CP Violation, and Rare Decays

After a >20-year search, D^0–$\overline{D}^0$ mixing is now established at >10 standard deviations [79, 80] (Fig. 8), thanks to the B factories and CDF. The level of mixing ($\sim 1\%$) is consistent with the wide range of Standard Model predictions [5]; however, this does not preclude a significant and potentially detectable contribution from new physics [32, 81]. Since some new-physics models predict differing effects in the charge-2/3 ("up-type") and –1/3 quark sectors [32, 81], it is important to carry out such studies not only with s and b hadrons, but with charm mesons as well — the only up-type system for which meson mixing can be measured.

While the total charm-production cross section for ≈ 8 GeV antiprotons incident on proton or nucleon targets is challenging to compute from first principles, recent phenomenological estimates imply values in the 1–10 μb range [82, 83, 84, 85, 86]. This is sufficiently large that the experiment we propose could amass a sample ten or more times larger than those of the B factories. For example, model-dependent calculations of the exclusive cross section $\sigma(\overline{p}p \to D^{*0}\overline{D}^0)$ peak at about 1 μb at $\sqrt{s} \approx 4.2$ GeV [84, 85, 86] (Fig. 9; see further discussion in Sec. 4.4.4). This corresponds to antiprotons of 8 GeV kinetic energy (the Antiproton Source design energy) impinging on a fixed target and, at $\mathcal{L} = 2 \times 10^{32}\,\mathrm{cm}^{-2}\mathrm{s}^{-1}$,

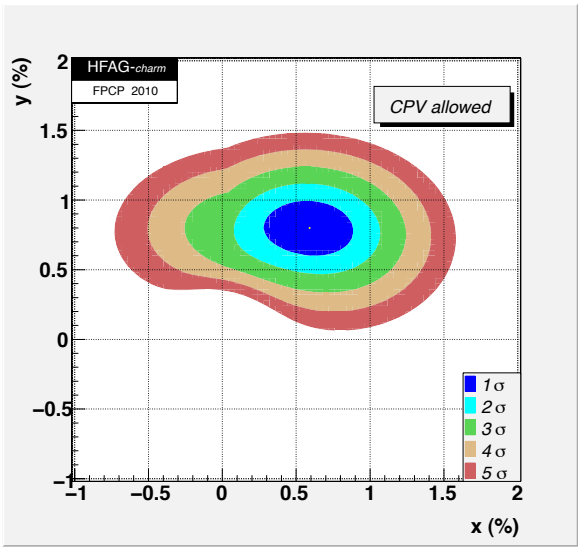

Figure 8: World average of D^0–$\overline{D}^0$ mixing parameters $x \equiv \Delta m/\Gamma$, $y \equiv \Delta\Gamma/2\Gamma$: best-fit values are $x = (0.59 \pm 0.20)\%$, $y = (0.80 \pm 0.13)\%$, and no mixing ($x = y = 0$) is disfavored by 10.2σ [79].

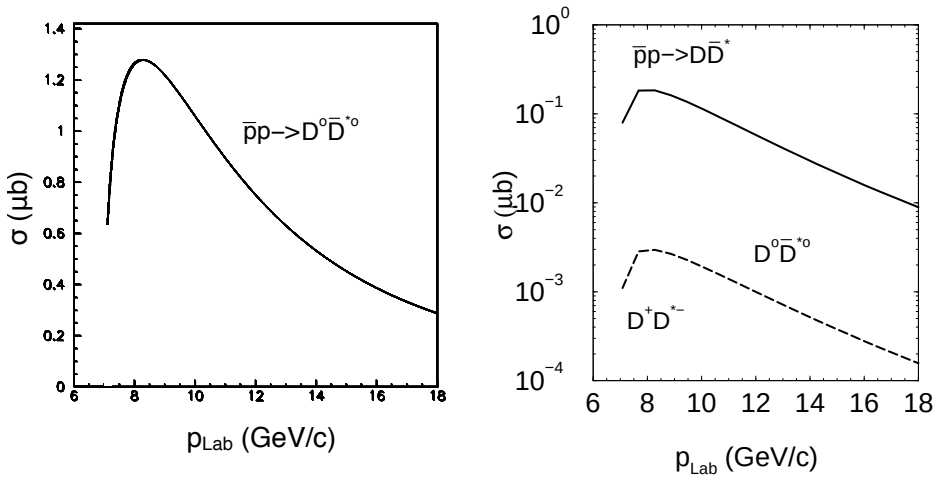

Figure 9: Total cross sections vs. antiproton momentum for $\overline{p}p \to D^0\overline{D}^{*0}$ (solid) and $\overline{p}p \to D^+\overline{D}^{*-}$ (dashed) from (left) Braaten formula (Eq. 11) [63] and (right) Regge calculation of Titov and Kämpfer [85, 86]. Given their uncertainties, these estimates are in agreement as to the order of magnitude of the cross section.

represents some 4×10^9 events produced per year. Since there will also be $D^{*\pm}D^{\mp}$, $D^*\overline{D}^*$, $D\overline{D}$, $D\overline{D}\pi$,... events, the total charm sample will be even larger, and with the use of a target nucleus heavier than hydrogen, the charm-production A-dependence [87, 88] should enhance statistics by a further factor of a few. The total sample could thus substantially exceed the 10^9 events produced at the B factories. Indeed, we project below in excess of 10^{10} tagged-D^0 events produced per year of running.

By localizing the primary interactions to $\sim 10\,\mu$m along the beam (z) direction, a thin wire or frozen-hydrogen target (or perhaps a small metallic pellet suspended on a low-mass stem) can allow the D-meson decay distance to be resolved. The low charged multiplicity

at these energies [19] implies small combinatorial background, so that clean samples can be amassed using only modest vertex cuts, and thus, with high efficiency. Medium energy $\bar{p}p$ or $\bar{p}N$ annihilation may thus be the optimal way to study charm mixing, and to search for possible new-physics contributions via the clean signature [15, 3, 32] of charm CPV.

4.4.1 D^0 mixing

Several signatures for charm mixing have been observed and indicate that charm mixing is at the upper end of the range expected in the SM [19]. These involve differing time-dependences of "right-sign" (RS) Cabibbo-favored and "wrong-sign" (WS) D^0 decays (arising both from doubly Cabibbo-suppressed decay and from mixing), differing lifetimes of decays to *CP*-even and mixed-*CP* final states, and Dalitz-plot analyses of 3-body D^0 decays. These processes are sensitive to various combinations of the reduced mixing parameters $x \equiv \Delta m/\Gamma$, $y \equiv \Delta\Gamma/2\Gamma$. As already mentioned, mixing at the observed level could be due to SM physics, but there could also be an appreciable or even dominant contribution from new physics, which could be indicated by *CP* violation.

The first publications of statistically significant signals for D^0–$\overline{D}^0$ mixing were from BABAR [89] and Belle [90] and employed $D^0 \to K^{\pm}\pi^{\mp}$ decays. Neglecting *CP* violation, for small mixing the ratio of the WS to RS decay rates is given by

$$R(t) = R_D + \sqrt{R_D}y'\Gamma t + \frac{x'^2 + y'^2}{4}(\Gamma t)^2 \,. \tag{6}$$

Here, R_D is the rate of the doubly-Cabibbo-suppressed (DCS) $D^0 \to K^+\pi^-$ decay, and x' and y' are "rotated" mixing parameters:

$$x' = x\cos\delta_{K\pi} + y\sin\delta_{K\pi} \,, \tag{7}$$

$$y' = -x\sin\delta_{K\pi} + y\cos\delta_{K\pi} \,, \tag{8}$$

where $\delta_{K\pi}$ is the strong phase difference between the DCS and Cabibbo-favored (CF) amplitudes. Sensitivity to small mixing arises from the second term on the right-hand side of Eq. 6, due to interference between DCS decay and mixing. RS and WS decays are identified using D^* tagging via $D^{*+} \to \pi_s^+ D^0$: RS decays have a slow pion, π_s, of the same sign as the pion from the D^0, while WS decays have the pion signs opposite each other. BABAR obtained $y' = [9.7 \pm 4.4\,(\text{stat}) \pm 3.1\,(\text{syst})] \times 10^{-3}$, with x' consistent with zero. Although the 1σ error gives the impression that this result is of marginal significance, BABAR found the no-mixing hypothesis to be inconsistent with their result by 3.9 standard deviations. CDF employed a similar technique, obtaining $y' = (8.5 \pm 7.6) \times 10^{-3}$, with no mixing disfavored by 3.8 standard deviations [91].

Belle observed a lifetime difference of $[1.31 \pm 0.32\,(\text{stat}) \pm 0.25\,(\text{syst})]\%$ between the CF decay to a mixed-*CP* state, $D^0 \to K^-\pi^+$, and the CS decays to *CP*-even states, $D^0 \to KK/\pi\pi$ [90]. This measures y_{CP} (= y in the limit of *CP* conservation):

$$y_{CP} = \frac{\langle\tau_{K\pi}\rangle}{\langle\tau_{hh}\rangle} - 1 \,, \tag{9}$$

where $\langle\tau_{hh}\rangle = (\tau_{hh}^{D^0} + \tau_{hh}^{\overline{D}^0})/2$ is the average lifetime of D^0 and $\overline{D}^0$ to K^+K^- and $\pi^+\pi^-$. BABAR subsequently used this technique as well, obtaining $y_{CP} = [1.24 \pm 0.39\,(\text{stat}) \pm 0.13\,(\text{syst})]\%$ for tagged [92] and $y_{CP} = [1.12 \pm 0.26\,(\text{stat}) \pm 0.22\,(\text{syst})]\%$ for untagged events [33].

In subsequent analyses, Belle [93] and BABAR [94] employed $D^0 \to K_S\pi^+\pi^-$ and $D^0 \to K_S K^+ K^-$ decays, comparing the Dalitz plots as a function of decay time for D^0 and $\overline{D}^0$. This technique (previously pioneered by CLEO [95]) has the virtue of measuring x and y directly, independent of strong phases. The Belle analysis gives $x = (0.80 \pm 0.29^{+0.09+0.10}_{-0.07-0.14})\%$ and $y = (0.33 \pm 0.24^{+0.08+0.06}_{-0.12-0.08})\%$ neglecting *CP* violation (the results allowing for *CP* violation differ only slightly from these).

These and other D-mixing measurements have been averaged by the Heavy Flavor Averaging Group (HFAG) [79] to obtain the results illustrated in Fig. 8. The no-mixing point ($x = y = 0$) is excluded at 10.2σ, x is nonzero at 3.2σ, and y is nonzero at 4.8σ. Since these mixing results are compatible with the high end of SM predictions, we turn to *CP* violation for possible evidence of new physics.

Three CPV parameters that may be extracted from these analyses are A_D, A_M, and ϕ, characterizing *CP* violation in decay, in mixing, and in interference between decay and mixing, respectively [96]. So far the CPV analyses are consistent with *CP* conservation, with limits on these parameters typically at the few-to-several-percent and several-degree levels. As an example, one of the best individual limits is $A_{CP}(K^*(892)^\mp\pi^\pm \to K_S\pi^+\pi^-) < 0.3\%$ in $D^0 \to K^{*-}\pi^+$, $\overline{D}^0 \to K^{*+}\pi^-$, from a Dalitz-plot fit by CLEO [97] using 4,854 events. Based on the assumptions of Table 5 (discussed in Sec. 4.4.4), we would expect more than 10^3 times as many events in our experiment, improving the limit to 0.90×10^{-4} or less, if both the statistical and systematic uncertainties scale as $\sqrt{N}$.

To summarize, given the kinematic similarities between the B factory D samples and that in our proposed experiment, we anticipate performing all of these mixing analyses with significantly greater sensitivity than has been achieved heretofore. (Systematic uncertainties typically have improved with increasing statistics.) For brevity we have omitted discussion of semileptonic D decays (in which to date significant mixing has not been observed), but our proposed experiment will measure them as well. Our sensitivity in semileptonic decays will depend on the efficiency and purity of lepton identification, which we have not yet simulated. In hadronic modes, we could be the world's most sensitive experiment, exceeding current B-factory statistics by a factor of 10 or more, and perhaps in semileptonic modes as well.

4.4.2 Direct CP violation

As mentioned above, there is sensitivity in charm mixing to direct as well as indirect CPV, but there can also be direct CPV that shows up independent of mixing, e.g., in partial-rate asymmetries of charged or neutral D's. Direct *CP* violation in charm decay is expected in the Standard Model at the $\sim 10^{-3}$ level [3], but only for singly Cabibbo-suppressed decays, for which tree and penguin diagrams can interfere, leading to partial-rate asymmetries:

$$A \equiv \frac{\Gamma(D \to f) - \Gamma(\overline{D} \to \overline{f})}{\Gamma(D \to f) + \Gamma(\overline{D} \to \overline{f})} \neq 0\,. \tag{10}$$

In the Standard Model, *CP* is conserved in CF and DCS charm decay, as there is only one type of SM diagram (the tree diagram) contributing to these modes. *Any* direct CPV in CF or DCS modes would thus be a clear indication of new physics [3]. Asymmetries in all three categories of decay modes could reach $\sim 10^{-2}$ in such scenarios as non-minimal supersymmetry [98] and left-right-symmetric models [99, 10]. For such an asymmetry to be observable, in addition to the weak phase difference, there must also be an appreciable strong phase difference; due to nearby resonances, there do seem to be large final-state

phases in a number of charm decay modes [3], favoring the observability of direct CPV via partial-rate asymmetries in charm decays.

Additionally, K^0 mixing leads to SM CP asymmetries of $\approx 2\mathrm{Re}(\epsilon_K) = 3.3\times10^{-3}$ in such modes as $D^+ \to K_S\pi^+$ and $K_S\ell\nu$ [100, 3], which should be observable in our experiment and could constitute a calibration for the experimental systematics of partial-rate asymmetries at the 10^{-3} level. Experimental partial-rate-asymmetry sensitivities have yet to reach this level [19].

Since partial-rate asymmetries can be faked by production asymmetries (even in $\overline{p}p$ collisions, given nonuniform solid-angle coverage), or by particle/antiparticle detection asymmetries due to differing π^+/π^- and K^+/K^- interaction cross sections in matter, it is important to have control signals. One approach is to use other signals, e.g., hyperon decay products and charged and neutral K's produced in association with hyperons (of which very large numbers will be available in this experiment), to calibrate the detection-efficiency asymmetries; more work will be required in order to evaluate the precision with which this calibration can be performed. Another approach is to look for partial-rate differences normalized to rates observed in CF modes, which is how this physics has been pursued in previous fixed-target experiments. For example, FOCUS [101] achieved a sensitivity of 0.14 in the DCS mode $D^0 \to K^+\pi^-$. The current best measurement in this mode, from BELLE [102], has a 1σ uncertainty of 0.047 based on 4024 events. This approach should allow sensitivity at or below the 3×10^{-3} level in our experiment. We note that such measurements are sensitive to new-physics mass scales very much higher than those directly probed at the LHC, recently estimated by Petrov as hundreds to thousands of TeV [103].

4.4.3 Rare charm decays

Another important benchmark for new-physics reach in charm is leptonic decays. An example is $D^0 \to \mu^+\mu^-$, whose branching ratio in the Standard Model has been estimated as $\sim\ 3 \times 10^{-13}$, but can be enhanced by new physics to as much as $\sim 4 \times 10^{-7}$ [3], possibly observable in BES-III as well as LHCb. The best current limit, 1.4×10^{-7} from Belle [104], thus already constrains SUSY models [105]. Our π/μ rejection will depend on how well the "picosecond" TOF detectors now under development [36] perform.

While $D^0 \to e^+e^-$ is helicity suppressed and extremely rare ($\mathcal{B} \sim 10^{-17}$ [16]) in the Standard Model, this suppression reflects the $V - A$ nature of the charged weak current, thus may well be absent if new physics plays a dominant role. As discussed above, we expect π/e rejection of order 10^{-5} per track. With (Table 5) over 2×10^{10} charm events produced and acceptance $\times$ efficiency ~ 0.05, our single-event sensitivity could approach 10^{-9}, surpassing the 3×10^{-8} (at 90% C.L.) estimated for BES-III [3]. Similar statements apply for other flavor-changing neutral-current, as well as lepton-number or -flavor-violating, modes such as $K\mu\mu$, Kee, $K\mu e$, etc. For all of these modes, the best limit from any approved experiment is expected to come from BES-III and to be statistics (not systematics) limited. In comparison, based on the assumptions used here, in each year of operation at 8 GeV our proposed experiment will amass over 27 times the statistics of BES-III.

A key background to $D^0 \to e^+e^-$ will of course be the Drell–Yan continuum discussed above, which at the D^0 mass represents some 10^6 events/GeV. A detailed simulation study to estimate how well the continuum can be rejected using D^*–D mass-difference and D^0 decay-vertex requirements would be desirable. However, it is unclear how to model soft pions produced in Drell–Yan events, which form the continuum background under the D^*–D^0 mass-difference peak. We show in Sec. 4.4.5 below based on preliminary MIPP data

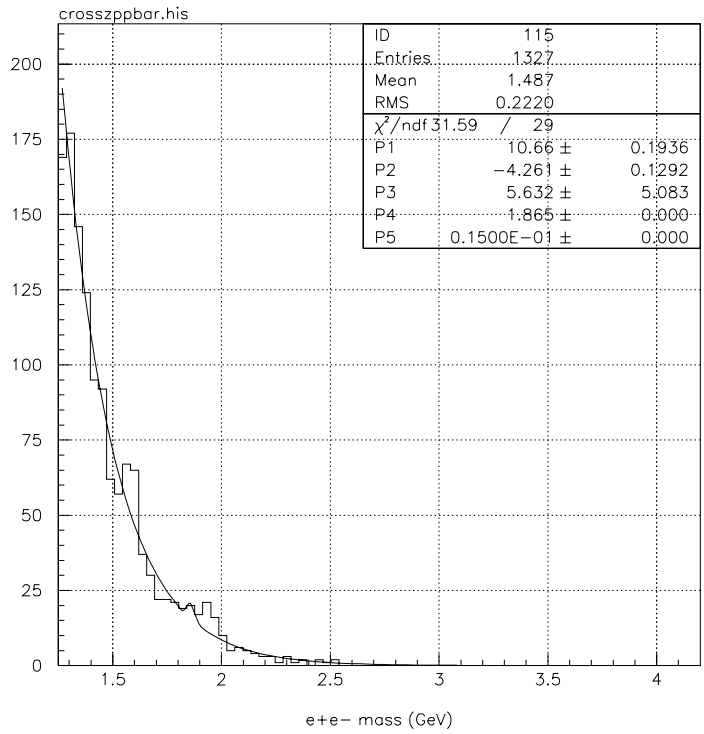

Figure 10: Histogram of Drell–Yan continuum after D^*–D^0 mass-difference and D^0 decay-vertex cuts as described in text, with exponential fit plus Gaussian representing $D^0 \to e^+e^-$.

that the pion-pair continuum under the $D^0 \to K\pi$ mass peak can be rejected by a factor of at least 50 by imposing the D^*-tag requirement, and that an additional factor of ~ 100 is available from decay-vertex cuts, while retaining signal efficiency $> 10\%$. This is also a plausible estimate for how well the Drell–Yan continuum under the $D^0 \to e^+e^-$ mas peak can be rejected. Requiring additional particles in the final state ($D^0 \to Kee$, ρee, etc.) can also help to reject continuum background. Figure 10 shows an example Monte Carlo mass spectrum of Drell–Yan e^+e^- events, assuming the rejection factors just stated, with an exponential-plus-Gaussian fit superimposed. The Gaussian function, representing the hypothetical $D^0 \to e^+e^-$ peak, has its mass constrained at $1.865\,\mathrm{GeV}/c^2$ and its width at $0.015\,\mathrm{GeV}/c^2$, per the Monte Carlo study described below. We see that in this instance the 1σ sensitivity is about 5 signal events, corresponding to a branching-ratio sensitivity of 5×10^{-9}. Repeating this exercise 10 times we find an average sensitivity of 4.2×10^{-9}, an order of magnitude better than projected for BES-III.

Another strength of TAPAS is the use of the E760/835 calorimeter to identify and reconstruct photons. This will give access to such modes as $D^0 \to \gamma\gamma$, $D^0 \to \rho\gamma$, etc., which due to combinatorics are hard to study at LHC*b*.

4.4.4 Charm cross-section and sensitivity estimates

An example sensitivity estimate, which should be compared with 1.2×10^6 tagged $D^0(\overline{D}^0) \to K^\mp\pi^\pm$ events observed in $0.54\,\mathrm{ab}^{-1}$ of data at Belle [90], is given in Table 5. It is based on

Table 5: Example sensitivity estimate for D^*-tagged $D^0 \to K\pi$ decays (after Ref. [63]). Note that the reliability of some of these values remains to be confirmed in detail. They are based on an exclusive cross-section estimate, so the inclusive production rate could be significantly higher, but the cross section, luminosity, or efficiency could also be lower. Hence, we show an indicative range of estimates.

Quantity	Value	Unit
Running time	2×10^7	s/yr
Duty factor	0.8*	
$\mathcal{L}$	2×10^{32}	$\mathrm{cm}^{-2}\mathrm{s}^{-1}$
Annual integrated $\mathcal{L}$	3.2	fb^{-1}
Target A	47.9	
$A^{0.29}$	3.1	
$\sigma(\bar{p}p \to D^{*+} + \text{anything})$	1.25–4.5	μb
# $D^{*\pm}$ produced	$(2.5\text{–}8.9) \times 10^{10}$	events/yr
$\mathcal{B}(D^{*+} \to D^0\pi^+)$	0.677	
$\mathcal{B}(D^0 \to K^-\pi^+)$	0.0389	
Acceptance	0.45	
Efficiency	0.1–0.3	
Total	$(0.3\text{–}3) \times 10^8$	events/yr

*Assumes $\approx 15\%$ of running time is devoted to antiproton-beam stacking.

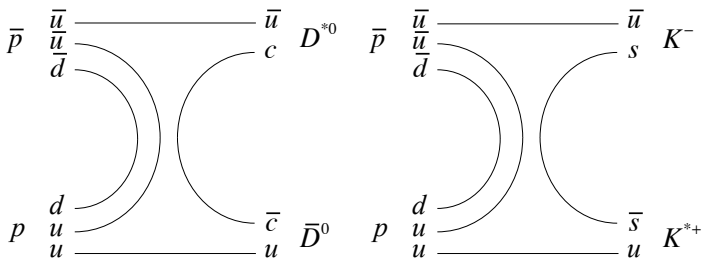

Figure 11: Comparison of leading Feynman diagrams for $\bar{p}p \to D^{*0}\overline{D}^0$ and $\bar{p}p \to K^{*+}K^-$; they differ only in the replacement of final-state charm quarks with strange quarks.

Braaten's formula [63],

$$\sigma[p\bar{p} \to D^{*0}\overline{D}^0; s] \approx \left(\frac{m_{D^*} + m_D}{\sqrt{s}}\right)^6 \frac{\lambda^{1/2}(s^{1/2}, m_{D^*}, m_D)}{[s(s-4m_p^2)]^{1/2}} \times (4800\,\mathrm{nb})\,, \tag{11}$$

where

$$\lambda(x,y,z) = x^4 + y^4 + z^4 - 2(x^2y^2 + y^2z^2 + z^2x^2)\,. \tag{12}$$

Equation 11 applies to the $D^{*0}\overline{D}^0$ exclusive final state, which however does not yield tagged D^0 decays, since the slow π^0 or gamma emitted in the D^{*0} decay to D^0 is not flavor-specific. To assess the reach in tagged-D^0 events, we must consider such exclusive final states as $D^{*+}D^-$, $D^{*+}D^{*-}$, $D^{*+}D^-\pi^0$, $D^{*+}D^0\pi^-$, $D^{*+}D^0\pi^-\pi^0$ (and charge-conjugate modes). Two-thirds of all D^{*+} decays are in the flavor-specific π^+D^0 mode, in which the charge of the slow pion tags the initial charm flavor of the D meson.

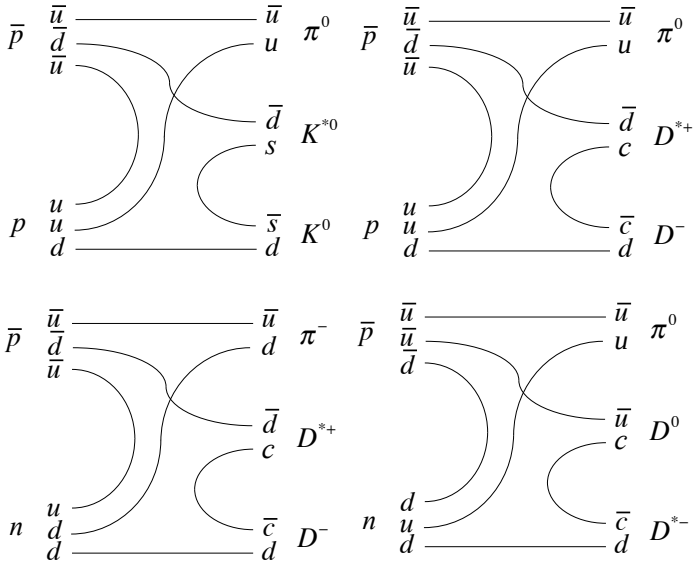

Figure 12: Some leading Feynman diagrams for $\overline{p}p \to K^*K\pi$, $\overline{p}p \to D^*D\pi$, and $\overline{p}n \to D^*D\pi$; note that compared with those of Fig. 11, these diagrams require only one pair of initial-state quarks to annihilate, thus may be less suppressed than those of Fig. 11.

Table 6: Various exclusive $\overline{p}p$ cross sections to final states containing K^{*0} (from [107]) at $\approx 750\,\mathrm{MeV}$ $\overline{p}$ kinetic energy. (Note that K_L was unobserved in [107]; we assume the cross sections for K_L and K_S are equal.)

Mode	σ (μb)	Error (μb)
$K^{*0}K_S$	150	20
$K^{*0}K_L$	150*	20*
$K^{*0}K_S\pi^0$	70	10
$K^{*0}K_L\pi^0$	70*	10*
$K^{*0}K^{\pm}\pi^{\mp}$	240	40
$K^{*0}\overline{K}^{*0}$	180	25
Sum	860	57

* assumed.

Braaten obtains Eq. 11 by relating the $\overline{p}p \to D^{*0}\overline{D}^0$ cross section to that for $\overline{p}p \to K^{*+}K^-$ (see Fig. 11), for which measurements are available from the Crystal Barrel experiment at LEAR [106] and from earlier bubble-chamber experiments [107]. This involves a kinematic extrapolation from well above threshold (where the exclusive cross section is an order of magnitude below its peak value) to the peak of the cross section. He estimates the uncertainty as a factor of 3 in either direction. Following his example, the best way to estimate the cross section for $D^{*\pm}$ production may be to relate it to measured $\overline{p}p$-annihilation cross sections to final states including K^{*0} (see Fig. 12). Some of these are available in Ganguli *et al.* [107]. As shown in Table 6, their sum of $(860 \pm 60)\,\mu$b substantially exceeds the size of the $K^{*+}K^-$ cross section as observed by Crystal Barrel, $(460 \pm 50)\,\mu$b, as well as that of Ganguli *et al.*, $(400 \pm 20)\,\mu$b. Since other final states containing K^{*0} are also possible besides those of Table 6, we take this as only a "subtotal"; i.e., the inclusive K^{*0}

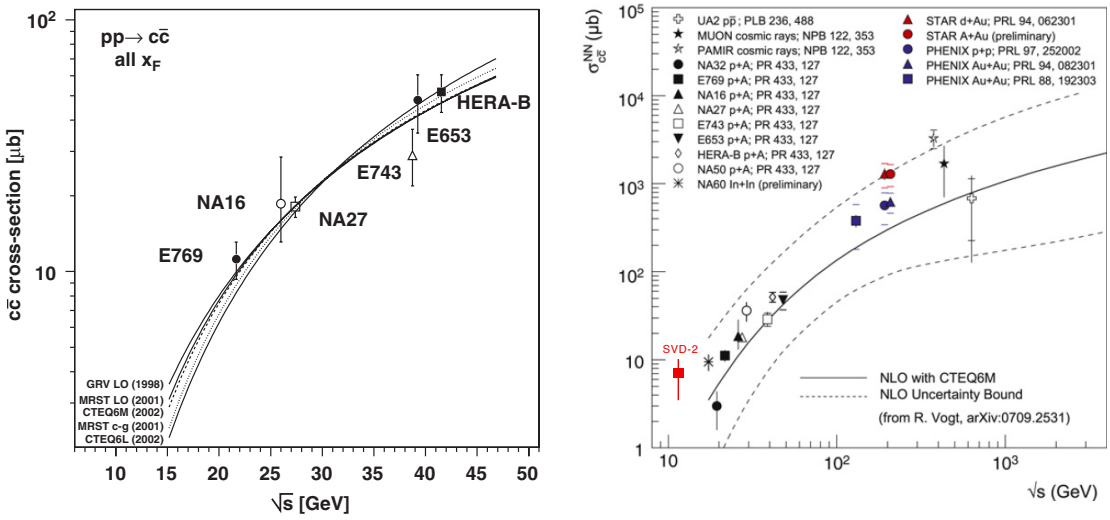

Figure 13: Total cross sections for $\overline{p}p \to c\overline{c}$ from (left) Ref. [88] and (right) Ref. [110] (after Ref. [109]).

cross section should be larger than this. Similarly, the inclusive D^{*+} cross section could be larger than estimated here, both because of additional final states and due to the extrapolation uncertainty in Braaten's formula. Thus a total charm cross section in 8 GeV $\overline{p}$ annihilation in the range 0.5–5 μb is not unlikely. (This does not take into account the further enhancement of the charm-to-total cross-section ratio due to A-dependence [87, 88].)

Additional cross-section estimates in the literature confirm the above range without reducing its uncertainty. Titov and Kämpfer [85] use a Regge approach, with the values of various free parameters determined from measured $\overline{p}p \to K\overline{K}$ and hyperon-antihyperon cross sections. Their focus on FAIR led them to consider in Ref. [85] 15 GeV/c antiprotons, rather than the 8.9 GeV/c which is the maximum $\overline{p}$ momentum at the Accumulator; however, Titov has recently provided [86] exclusive total $D\overline{D}^*$ cross-section predictions vs. antiproton momentum, shown in Fig. 9(right). For $D^0\overline{D}^{*0}$ these are lower than obtained using Braaten's formula by a factor of 6. (Given the uncertainties of low-momentum-transfer, non-perturbative QCD, Braaten views this as agreement with his estimate [108].)

Lourenço and Wöhri have surveyed the charm-production literature [88]. As suggested by Fig. 13, the extrapolation from the 210 GeV pp data of E769 down to 8.9 GeV $\overline{p}p$ is fraught with uncertainty, and this uncertainty is not reduced by the QCD parametrizations shown on the figure. Also shown in Fig. 13 are results from a more recent compilation by Frawley, Ullrich, and Vogt [109], as updated with an additional data point from the 70 GeV SVD-2 experiment performed at Serpukhov [110] — the lowest energy for which pN charm cross sections have been published. The SVD-2 result, $\sigma = 7.1 \pm 2.4 \pm 1.4\,\mu$b/nucleon, seems to imply a low-energy trend rather different from that of the QCD extrapolations — hardly surprising, since the behavior of the cross section near threshold is unlikely to be captured by perturbative calculations. Indeed, the lowest-energy cross-section values seem to be falling with decreasing energy more slowly than predicted by perturbative QCD. This is one more piece of supporting evidence for $\sim \mu b$ charm production in 8 GeV antiproton annihilation.

Table 7: Key parameters of simulated detectors.

Parameter	Value	Unit
Target (D study):		
material	Al	
configuration	wire	
diameter	30	μm
Target (X study):		
material	H_2	
configuration	cluster jet	
Beam pipe:		
material	Be	
diameter	5	cm
thickness	350	μm
Solenoid:		
length	1.6	m
inner diameter	90	cm
field	1	T
SciFi detectors:		
total thickness per doublet	360	μm
fiber pitch	272	μm
fiber diameter	250	μm
number of stations	8	
number of views	3	
number of channels	≈90,000	

Table 8: Detector positions used in simulations (target is at $z = 0$). All detector planes assumed to cover 2.54 to 40.6 cm in radius.

SciFi station	z	Unit
1	8.76	cm
2	20.83	cm
3	36.19	cm
4	54.86	cm
5	76.83	cm
6	102.11	cm
7	130.68	cm
8	162.5	cm

4.4.5 Charm Monte Carlo and background studies

We have carried out simulations of charm events with the apparatus of Fig. 1(left); key parameters of the simulation are given in Tables 7 and 8. In particular we studied $\overline{p}n \to D^{*-}D^0$, with subsequent decays $D^{*-} \to \pi_s^- \overline{D}^0$, $\overline{D}^0 \to K^+\pi^-$, for which we find the D^{*-} geometric acceptance to be 45%, with ≈ 0.75% mass resolution and 0.46 MeV/c^2 resolution on the D^*–D mass difference. Figures 14–17 show some results from the charm Monte Carlo study, indicating r.m.s. resolutions in D^* and D^0 mass and D^*–D^0 mass difference of 14.9, 14.9, and 0.46 MeV/c^2, respectively, and vertex z resolution of 150 μm.

We do not expect Monte Carlo simulations to be reliable for estimation of the combinatoric (continuum) background under the D peak. To estimate the combinatoric background, we therefore rely on a preliminary analysis of events from the MIPP experiment [111], using a 20 GeV $\overline{p}$ beam (the lowest energy for which a useful amount of data was available) and scaling the laboratory-frame longitudinal momenta of all secondaries by a factor 0.65 to approximate the effect of running at 8 GeV.[8] We searched the MIPP data sample for events containing three charged hadrons, two of one sign and one of the other, consistent with being decay products of a $D^{*+} \to \pi_s^+ D^0$, $D^0 \to K^-\pi^+$ or $D^{*-} \to \pi_s^- \overline{D}^0$, $\overline{D}^0 \to K^+\pi^-$ decay

[8]The lab-momentum scale factor was determined by comparing the longitudinal-momentum distributions from Monte Carlo simulations of D^* production and decay at 20 GeV and 8 GeV beam energies; we note that it is close to the ratio of $\sqrt{s}$ at the two energies. This procedure is conservative in that it neglects the reduction in charged-particle multiplicities and transverse momenta at 8 GeV compared to 20 GeV.

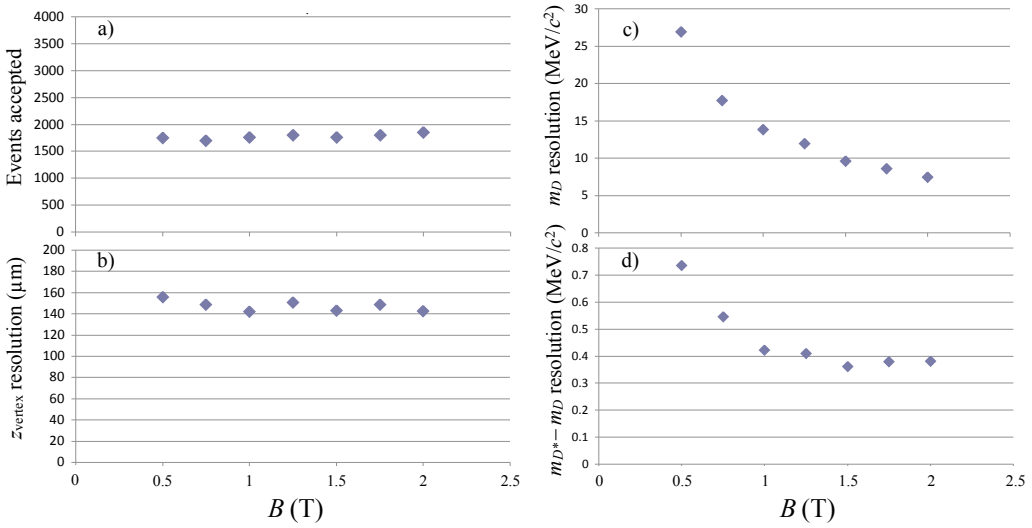

Figure 14: Magnetic-field dependence of a) number of events accepted (out of 4,000 thrown), b) decay-distance resolution, c) D^0 mass resolution, and d) D^*–D^0 mass-difference resolution. Above ≈ 1 T, spectrometer performance improves only slightly.

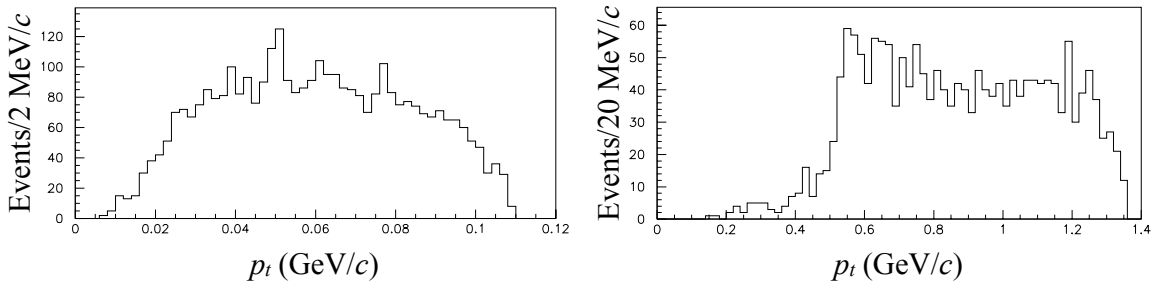

Figure 15: Transverse-momentum (p_t) histograms for charged pions from accepted tagged-D^0 events. The "slow" (left histogram) and "fast" pions (right histogram) are seen to have non-overlapping p_t distributions, thus there is no ambiguity in event reconstruction as to which is which. (The p_t distribution of the kaon is similar to that of the fast pion.)

sequence. We find 1.1 ± 0.3 such events within the 2σ D^0 mass and D^{*+}–D^0 mass-difference windows (see Fig. 18), corresponding to a continuum cross section of approximately 1 μb, before hadron-ID and vertex cuts. (Note that this MIPP sensitivity is far from what is needed to see actual charm decays, since the $D^{*+} \to D^0\pi^+$ and $D^0 \to K^-\pi^+$ branching ratios — 0.677 and 0.0389, respectively [19] — mean that for a 1 μb D^{*+} cross section, only 0.05 events would be expected. However, it suffices for an estimate of the continuum background under the D^0 peak.)

We can then estimate the D^*-tagged $D^0 \to K^-\pi^+$ signal-to-background ratio as follows:

- For the purposes of this estimate, per Table 5, we take the sum of inclusive D^{*+} and D^{*-} cross sections in 8 GeV $\overline{p}$-Ti collisions to be $2 \times 1.25\,\mu\text{b} \times 47.9^{0.29} = 7.7\,\mu\text{b}$.
- Applying the product branching ratio for the $\pi_s^+ K^-\pi^+$ final state, we have a signal cross section $\times$ branching ratio of 0.2 μb.
- The corresponding continuum background under the D^0 peak is (per the discussion

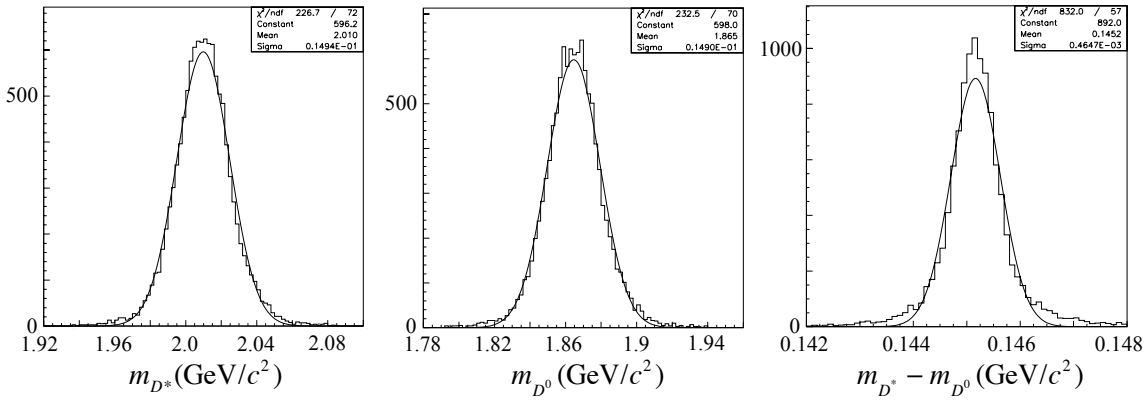

Figure 16: (left to right) Histograms of D^* and D^0 mass, and D^*-D^0 mass difference, indicating r.m.s. resolutions of 14.9, 14.9, and 0.46 MeV/c^2, respectively.

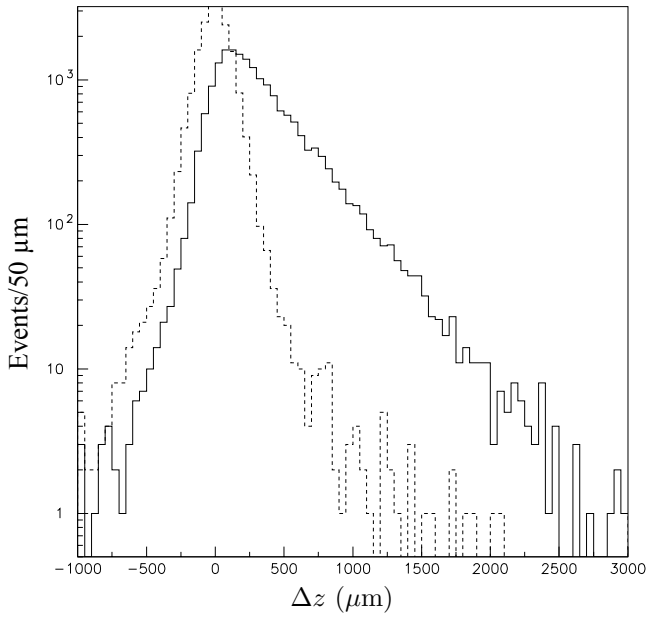

Figure 17: Monte Carlo simulation of D^0 decay-vertex distribution (solid histogram) as reconstructed in 272-μm-pitch scintillating-fiber detectors, compared with that of random hadron pairs (dashed histogram).

above) $\approx 1.1\,\mu$b, giving a signal-to-background ratio before analysis cuts of 20%.

- The continuum background estimate, however, corresponds mostly to misidentified $\pi^\pm\pi^\mp\pi^\pm$ events,[9] and since only about 6% of 8 GeV $\overline{p}p$ interactions have charged kaons [112, 113], we estimate a signal-to-background ratio of about 7-to-1 before vertex cuts.

As mentioned above, with an all-SciFi tracker we find 150 μm resolution in decay-vertex z (Fig. 17), while the mean D^0 decay distance is 325 μm, allowing $\sim$100-to-1 signal-to-

[9] We did not attempt to use the MIPP hadron-ID detectors due to the events being in a difficult momentum range for those detectors.

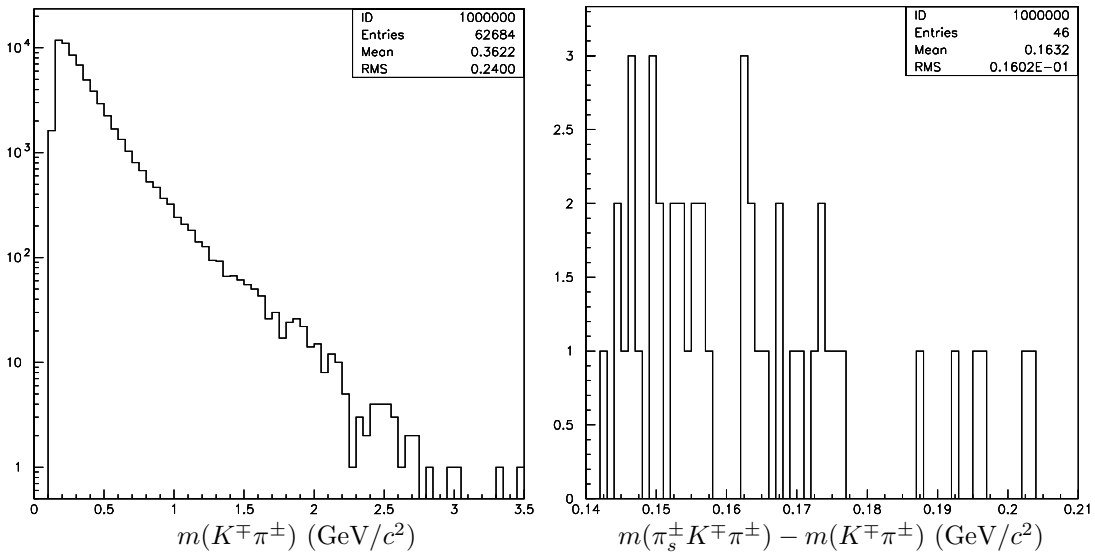

Figure 18: (Left) Histogram of reconstructed $K^{\mp}\pi^{\pm}$ mass (in GeV/c^2) from MIPP analysis; (right) histogram of reconstructed D^*-D mass difference (in GeV/c^2) for MIPP events with $K^{\mp}\pi^{\pm}$ mass within 2σ of D^0: signal bin is $|m(\pi_s^{\pm}K^{\mp}\pi^{\pm}) - m(K^{\mp}\pi^{\pm}) - 0.1455\,\mathrm{GeV}/c^2| < 0.92\,\mathrm{MeV}/c^2$.

background after vertex cuts with efficiency $>10\%$. For example, with a $300\,\mu$m z-vertex cut, which is 50% efficient, the signal-to-background ratio is 30-to-1. This signal-to-background calculation is summarized in Table 9. (We have conservatively estimated a 10% efficiency in Tables 5 and 9 to take account of other cuts and inefficiencies as well.) In particular, by conservatively assuming the low end of the parameter range of Table 5, we could expect to reconstruct 2.8×10^7 tagged $D^0 \to K^-\pi^+$ events per year, to be compared with 1.2×10^6 events in the largest published sample to date [90], based on $540\,\mathrm{pb}^{-1}$ of data taken at Belle.[10]

Table 9: Illustrative signal-to-background estimate for D^*-tagged $D^0 \to K\pi$ decays.*

Quantity	Value	Unit
Signal $\sigma \cdot \mathcal{B}$	0.2	μb
$\sigma(\pi^{\pm}\pi^+\pi^-)$ under $D^{*\pm}$ peak	1.1 ± 0.3	μb
Signal-to-background ratio before cuts	≈ 0.2	
π/K rejection	$0.06/2 = 0.03^{\dagger}$	
Vertex rejection	0.02	
Signal efficiency	10%	
Signal-to-background ratio after cuts	≈ 30	

*Conservative values from Table 5 chosen, corresponding to $\approx 3 \times 10^7$ signal events/yr.

†Factor 2 reduction in background combinatorics from knowing which hadron is the kaon.

(It is worth noting here that the role of kaon identification in this analysis is to im-

[10]We also note that the Belle result — a $D^0 \to K\pi$ vs. $D^0 \to KK/\pi\pi$ lifetime difference of $(1.31 \pm 0.32 \pm 0.25)\%$ — has comparable statistical and systematic uncertainties. Thus the precision in a super-B factory may well not improve with increased statistics by as large a factor as naively expected.

prove the signal-to-background ratio in order to allow sensitive measurements of mixing and searches for CPV, whereas the charm production cross section can be measured without hadron-ID. In this scenario, each $K\pi$ candidate event is entered twice in the mass histogram, once as $K^-\pi^+$ and once as $K^+\pi^-$. The correctly identified events will form a narrow peak, above a broad background of incorrectly identified ones; this approach works also for other decay modes. Thus, if necessary, the TOF counters can be added as an upgrade subsequent to the start of data taking, as discussed in Sec. 5.5. The TOF detectors play a larger role in the charm running than in hyperon or $X(3872)$ running, where there are sufficient kinematic constraints to identify secondaries correctly without PID information.)

4.5 Additional Physics

The proposed experiment will be relevant to many topics besides the main ones described above, providing the opportunity for several dozen additional physics papers and thesis topics. Here we briefly summarize a few examples.

As mentioned above, very little is known about 3.5–8 GeV antiproton interactions. We will measure for the first time particle multiplicities and differential cross sections with precision over the full range of beam energy accessible at the Accumulator. This is of particular interest for the $\overline{\mathrm{P}}$ANDA experiment at FAIR, whose trigger and data-acquisition systems are now being designed based on Monte Carlo models of minimum-bias cross reactions, whose reliability is difficult to ascertain. Such measurements can also be used to test models of non-perturbative QCD.

It has been suggested [108, 34] that the $X(3872)$ may be for $\overline{p}p$ annihilation what the $\psi(3770)$ is for e^+e^- annihilation: a source of quantum-correlated charmed-particle pairs affording good sensitivity to charm mixing parameters. Depending on the width and formation cross-section of the $X(3872)$, this may be competitive with BES-III.[11] If the X is in fact a tetraquark state rather than a molecule, there may also be a partner state, with 0^{++} quantum numbers (hence inaccessible to e^+e^-), at $\approx 40\,\mathrm{MeV}/c^2$ lower mass [114], decaying to $D\overline{D}$, which might also serve this purpose.

The analysis of hyperon transverse-momentum distributions, dN/dp_t, gathered from various experiments (WA89, ISR, STAR, UA1, and CDF) reveals an important difference in the dynamics of multiparticle production in proton-proton vs. antiproton-proton collisions [115] (see Fig. 19). Hyperons produced with proton beam display a sharp exponential slope at low p_t, while those produced with antiproton beam do not. Since LHC experiments have proton projectiles, the spectra of multiparticle production at LHC should seem "soft" in comparison to predictions, because the MC predictions were based on Tevatron (antiproton) data. From the point of view of the Quark-Gluon String Model [116], the most important contribution to particle production spectra in antiproton-proton reactions is due to antidiquark-diquark fragmentation. Measurements of p_t spectra in antiproton-proton interactions at a variety of energies can thus constrain the contribution from the fragmentation of antidiquark-diquark strings. This study may have impact not only on the interpretation of LHC results, but also on cosmic-ray physics and astrophysics where matter-antimatter asymmetry is being studied.

[11] If the $X(3872)$ turns out to be extremely narrow, as expected in the molecular hypothesis, taking full advantage of this option would require additional antiproton cooling in order to narrow the beam-energy distribution and increase the $X(3872)$ formation rate compared to production of continuum events; this could be accomplished by installing the Recycler electron-cooling system in the Accumulator, which is however beyond the scope of the currently proposed effort.

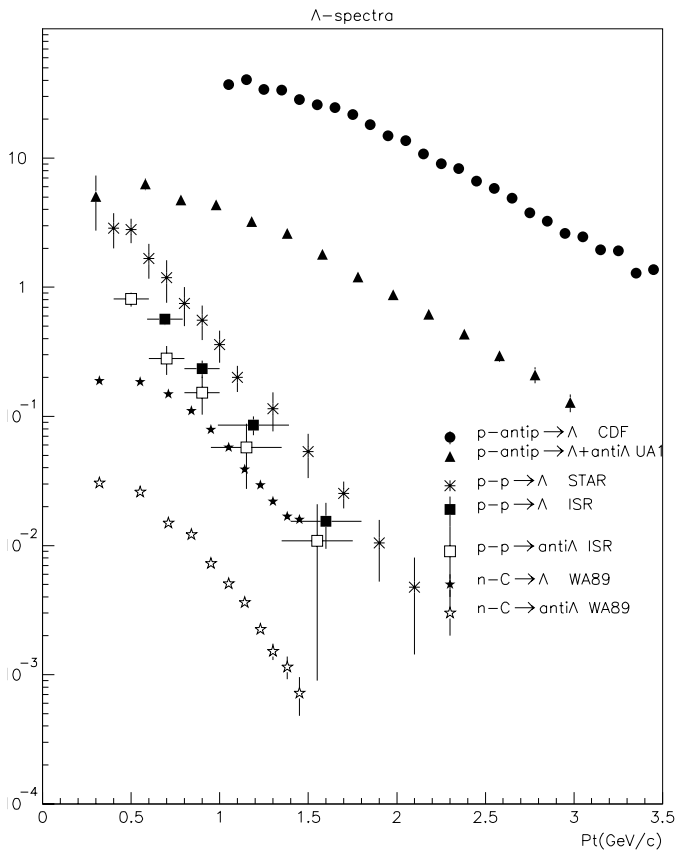

Figure 19: Data on Λ p_t spectra (in arbitrary units) from WA89 [117], ISR [118], STAR [119], UA1 [120], and CDF [121] show systematically different exponential slopes between proton and antiproton beams.

The experiment will also have useful sensitivity to possible exotic states. An example is the pentaquark, first discussed by Lipkin [122], who pointed out that the "anti-charm strange baryon" ($\bar{c}uuds$ or $\bar{c}udds$) could be more strongly bound than the H (di-Lambda) proposed by Jaffe [123]. While these remain a controversial topic and the subject of many recent papers [124], the question of stability of >3-quark states is of substantial intrinsic interest, akin to the possible molecular nature of the $X(3872)$. Although there are upper limits on their production cross section times branching ratio to $\phi\pi p$ or K^*Kp [125], Lipkin's pentaquarks are by no means entirely ruled out. One by-product of the charm mixing and CPV search discussed above will be improved sensitivity to charmed pentaquarks. We will thus set new limits on (if not discover) the anti-charm strange baryon and shed new light on this (to date) vexing question.

Several X, Y, and Z states besides the $X(3872)$ have been observed at the B factories (some of which are discussed in [2]). Our understanding of these could benefit from $\overline{p}p$ formation or production studies. Many, though not all, are accessible at Accumulator energies: the $X(3940)$, $X(4140)$, $X(4260)$, $Y(3940)$, $Y(4260)$, and $Z(3930)$ [2, 19]. Some may not be distinct states and some may be charmonium states, but their study in $\overline{p}p$ could yield valuable information.

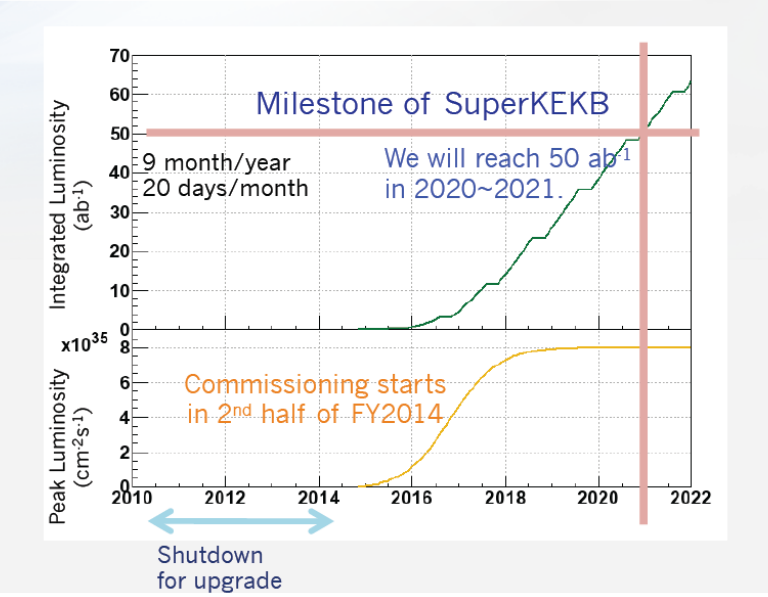

Figure 20: Integrated luminosity vs time projected for Belle II at SuperKEKB [126]. SuperB is likely to start later but aims for similar reach.

4.6 Competition

Over the next several years, LHC*b* will obtain the largest charm samples of any approved experiment. In the longer term, by the early 2020s the "super" B factories will integrate sufficient luminosity to become competitive (Fig. 20), with $\approx 1 \times 10^8$ tagged, reconstructed $D^0 \to K^-\pi^+$ events.

LHC*b* is now publishing their first charm results, which (since they are already operating at $3 \times 10^{32}\,\mathrm{cm}^{-2}\mathrm{s}^{-1}$, 50% beyond their design luminosity) are indicative of their reach in future years. G. Wilkinson's LHC*b* talk at the EPS 2011 meeting [127] reports a 6.5 mb charm cross section, suggesting that LHC*b* charm statistics will be enormous. However, they are in fact rather inefficient at recording and reconstructing charm decays — a necessary consequence of their limited angular coverage and data-acquisition bandwidth, together with the short D-meson lifetimes, which make their secondary-vertex trigger algorithms inefficient for charm.

Specifically, Wilkinson presents [127] a histogram of D^*-tagged, reconstructed $D^0 \to K^+K^-$ decays (reproduced in Fig. 21) from $195\,\mathrm{pb}^{-1}$ of LHC*b* data. This decay chain has a combined 2.6×10^{-3} branching ratio. The cuts chosen leave significant background under the peak, which we can take into account by derating their statistics by the factor $N/(\delta N)^2 = 679,200/1200^2 = 0.47$. Given the quoted cross section and integrated luminosity, their produced charm sample is some 1.2×10^{12} events. With the $\sim 10\%$ TAPAS acceptance $\times$ efficiency presented above, one would thus expect $\sim 10^8$ tagged, reconstructed events in this mode, where their sensitivity is in fact $7 \times 10^5 \times 0.47 = 3 \times 10^5$ events. Their acceptance $\times$ efficiency for these charm modes is thus only $\sim 10^{-4}$.

By 2016, given the long LHC repair shutdown, LHC*b* is expected to amass some $5\,\mathrm{fb}^{-1}$ of data. Extrapolating from Wilkinson's EPS 2011 talk, the equivalent sample in tagged $D^{*\pm} \to (K\pi)\pi$ will be $\approx 4 \times 10^7$ events. (By trigger optimization they may gain an additional factor of ~ 2.) This should be compared with (0.3–3) $\times 10^8$ events/yr in Table 5 above, which

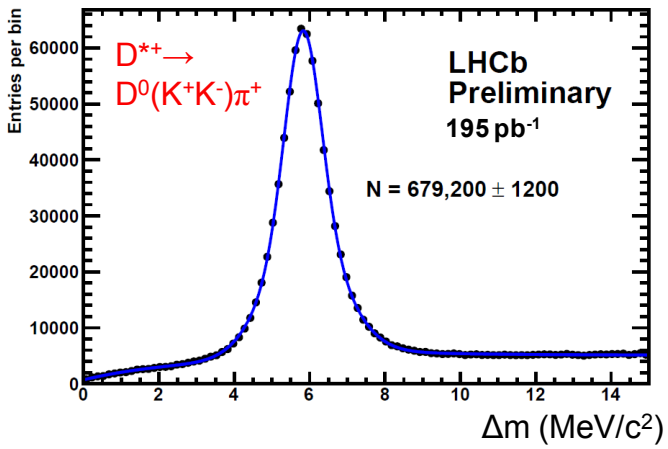

Figure 21: Tagged D^0 decays from the sequence $D^{*+} \to D^0\pi^+, D^0 \to K^+K^-$, as reconstructed by LHC*b* in 195 pb^{-1} of data [127].

indicates that LHC*b* is likely to have an integrated charm sample by 2016 that is at the low range of expectations for TAPAS. We thus anticipate competing quite effectively with LHC*b*, as well as beating Belle II and SuperB to the punch by several years.

For the hyperon, charmonium, "XYZ," and Drell–Yan measurements discussed here, the only competition is the $\overline{\text{P}}$ANDA experiment [82] under development for operation with antiprotons in the FAIR "high-energy" storage ring (HESR). Fermilab can implement the TAPAS experiment some years before the HESR at FAIR is likely to be in operation, and many years before it reaches full intensity. While the large and comprehensive $\overline{\text{P}}$ANDA spectrometer will be a superior general-purpose detector, for the focused program of physics investigations we propose, it has little advantage over the apparatus we propose to assemble.

5 Experiment Description

5.1 Beam

We will use the Antiproton Accumulator beam, with no modification of the facility required other than replacement of a short length of beam pipe at AP-50. In particular, use of the Recycler is not required, thus the proposed TAPAS program is not in conflict with the proton-beam intensity upgrade planned for NOνA. In order to avoid scattering secondaries more than necessary as they enter the detector, we will employ a thin beryllium beam pipe. There are leftover beam pipes from DØ and CDF that appear to be suitable and are already available on the shelf without disassembly of those experiments.

Antiproton cooling and accumulation will be performed in the Accumulator. The assumed initial beam current is 50–100 mA, which can be accumulated (without use of the Recycler) in $\approx$2.5–5 hours at 20 mA/hr; stacking will thus occupy $\approx$10–20% of operating time. For running at antiproton kinetic energies below 8 GeV, some time will also be required for deceleration. This is accomplished using an RF cavity operating at the second harmonic of the beam revolution frequency, with a maximum RF voltage of about 3 kV, allowing a deceleration rate of about 20 MeV/s [37].[12] Depending upon the desired beam

[12]Deceleration of course relies on the beam being bunched to some degree, as does precision calibration of the beam orbit length (and hence, energy) using beam position monitors (BPMs). This is in tension with

energy, we expect the useful beam lifetime to be 10–20 hours.

A nominal run plan could consist of a day-long cycle of stacking, beam preparation, data taking and recovery. We can expect to achieve $\approx 8\,\mathrm{pb}^{-1}$ per day and $> 200\,\mathrm{pb}^{-1}$ per month. The r.m.s. spread of the center-of-mass energy in E835 was $\approx 300\,\mathrm{keV}$ [37], allowing measurement of resonance widths with $\lesssim 100\,\mathrm{keV}$ precision. Using the ψ' mass (known to $0.04\,\mathrm{MeV}$ [19]) as calibration point, E835 achieved an r.m.s. uncertainty of $\leq 0.15\,\mathrm{MeV}/c^2$ in the measurement of charmonium-state masses [37]. We anticipate similar performance in this experiment.

Currently, the Main Injector minimum cycle time is set at 2.2 seconds to load protons and ramp. In the NOνA era, the Recycler Ring will provide protons in one turn and then the minimum Main Injector (MI) cycle time will just consist of the ramp: 1.33 seconds. The Antiproton Source is not capable of running at that cycle time and would therefore take two out of twelve MI batches of proton beam on target every other MI cycle. We note that during stacking there will be a small impact on the beam intensity available to NOνA, given by $1/2 \times 2/12 = 8.3\%$. Since this will occur at most 20% of the time, the integrated effect on NOνA will be less than 2%.

5.2 Targets

Of the physics topics proposed above, some require a hydrogen target while others may be optimized by the use of a nuclear target. The hydrogen cluster-jet target used in E835 is currently at GSI Darmstadt, where it has been used in prototype studies for development of the $\overline{\mathrm{P}}$ANDA target, but it can be returned to Fermilab and made available for our experiment if we so request [129]. We are also proposing to use wire (or pellet) targets of various materials (for example, Be, Al, and Ti), which can localize the primary vertices in two or three dimensions and thus aid in the identification of charm decays. Development of a movable wire or pellet target is a rather small job which could be carried out at Fermilab or by a collaborating group.

As discussed above, the study of the properties of the $X(3872)$ calls for a hydrogen target in order to minimize the spread in collision energy. However, the X includes D mesons among its decay products, whose detection would benefit from a thin target. A frozen-hydrogen target could bring the advantage of localizing the primary vertices (not possible with a gas jet) without the drawback of windows, which a liquid-hydrogen target would entail. By providing a known initial state having minimal energy spread, a hydrogen target could also be advantageous for charm running, providing a constraint that can be used for particle ID. Whether this outweighs the cross-section advantage of nuclear targets can probably be reliably assessed only with actual data.

We next discuss in greater detail each of the three options just mentioned. In each case, the thickness of the target should be such as to give the desired $\approx 10\,\mathrm{MHz}$ inelastic-interaction rate at the intended rate of circulating antiprotons. The 50–100 mA circulating beam current discussed above represents $(0.5 \text{ to } 1)\times 10^{12}$ antiprotons stored in the 474-m-circumference Accumulator ring. Thus the rate at which antiprotons circulate past the target is $R = (3 \text{ to } 6) \times 10^{17}\,\overline{p}/\mathrm{s}$.

the need for a debunched beam in order to maximize the rate of stochastic cooling. The compromise solution described here is the one successfully devised for E835 [37].

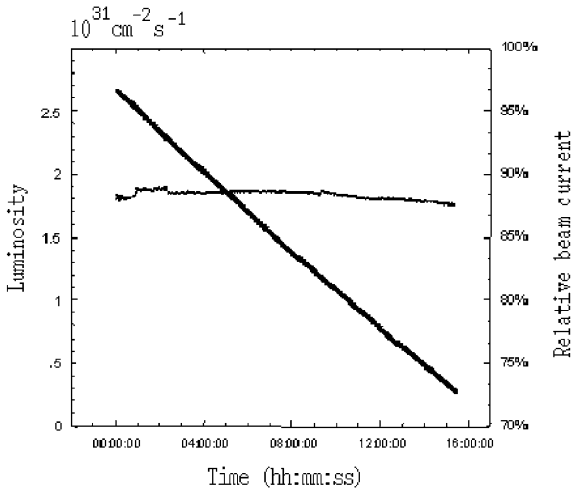

Figure 22: Illustration of luminosity leveling achieved in E835 (from [37]).

5.2.1 Cluster-jet target

E835 employed a hydrogen cluster-jet target, and a similar target is in preparation for $\overline{\mathrm{P}}$ANDA. The maximum target density achieved in E835 was 3.2×10^{14} atoms/cm^3 [37], which the $\overline{\mathrm{P}}$ANDA collaboration projects can be improved so as to reach a luminosity of $2 \times 10^{32}\,\mathrm{cm}^{-2}\mathrm{s}^{-1}$. An advantage of the cluster-jet technique is the ability to control the target density precisely and vary it over the course of the fill so as to do "luminosity leveling" as the circulating beam is depleted. This ability depends on having some head room, i.e., being able to achieve a higher target density than needed at the initial beam intensity. As shown in Fig. 22, in E835 this was successfully accomplished at luminosities up to $\approx 2 \times 10^{31}\,\mathrm{cm}^{-2}\mathrm{s}^{-1}$ [37].

At a beam intensity I_B and jet diameter d_J, the jet density needed for a given luminosity $\mathcal{L}$ is

$$\rho \approx \frac{\mathcal{L}}{I_B d_J}\,. \tag{13}$$

For $I_B = 6 \times 10^{17}\,\mathrm{s}^{-1}$, $\mathcal{L} = 2 \times 10^{32}\,\mathrm{cm}^{-2}\mathrm{s}^{-1}$, and $d_J = 0.6\,\mathrm{cm}$ as in E835, we obtain $\rho = 6 \times 10^{14}\,\mathrm{atoms/cm}^3$, about a factor 2 higher than achieved in E835 [37]. For luminosity leveling, some headroom beyond this would be desirable. It is likely that this density increase can be accomplished, as envisioned by $\overline{\mathrm{P}}$ANDA [38]. However, since many of our physics goals benefit from a short target, our baseline hydrogen target is the frozen-hydrogen target described below.

5.2.2 Wire target

A wire target is straightforward and will take little effort to prepare, using standard, off-the-shelf Fermilab modules. A thin wire will be stretched across, and attached to, a fork mounted within the beam pipe, such that it can be moved towards or away from the beam via a stepping motor. (Alternatively, a small pellet can be affixed to a thin, low-mass support, e.g., a 100-μm-diameter Ti pellet fastened to a $10\,\mu$m Ti wire.) Given the magnetic field at the target location, the motor will likely be pneumatically actuated. During antiproton stacking, the wire will be parked far from the beam. Once a stable, cooled beam

is circulating, the fork will be carefully moved inwards until the desired interaction rate is reached. At present it is unclear whether the beam halo will be spontaneously replenished, such that a constant wire position will result in a constant interaction rate, or whether the wire will clean out and deplete the halo. In the latter case, the wire can gradually be moved further inwards to maintain a constant interaction rate, or halo can be artificially generated by injecting a small amount of noise into the stochastic-cooling system.

As an example, the nuclear interaction length of titanium is $\lambda_I = 27.5\,\mathrm{cm}$, thus a 30-$\mu$m-thick titanium slab would represent $0.01\%\,\lambda_I$ [19]; taking into account its cylindrical cross section, a 30-μm-diameter Ti wire thus has an average thickness in interaction lengths $t = 8.6 \times 10^{-5}\,\lambda_I$. Thus to sustain an interaction rate $R_I = 10\,\mathrm{MHz}$ will require a rate of antiprotons hitting the target given by

$$R_{\overline{p}} = \frac{R_I}{t} = \frac{10\,\mathrm{MHz}}{8.6 \times 10^{-5}} = 1.2 \times 10^{11}\,\mathrm{Hz}\,. \tag{14}$$

Compared to the circulating antiproton rate, this is somewhat less than 1 antiproton per million. Approximating the transverse beam distribution in x or y as Gaussian, the target would need to be maintained about 3.5 standard deviations out from the beam center.

The rate of ionization energy loss for antiprotons traversing such a target averages $dE/dx \times t_{avg} = 7.0\,\mathrm{MeV/cm} \times \pi d/4 = 1.6\,\mathrm{keV}$ per crossing. The radiation length of Ti is $X_0 = 3.56\,\mathrm{cm}$, so the target represents $0.068\%\,X_0$, thus the mean-square multiple-scattering angle of traversing antiprotons is increased at the rate $\approx (14\,\mathrm{MeV}/c\,/\,p)^2\,(x/X_0) = (1.7\,\mathrm{nrad})^2$ per crossing at 8 GeV. The stochastic-cooling system should be capable of compensating for these small effects, in order to maintain approximately constant beam energy spread and divergence and minimize beam loss. Some experimentation with wires of various materials will be required to ascertain which target material is optimal in this regard.[13]

5.2.3 Frozen-hydrogen target

Ishimoto *et al.* at KEK have successfully built and operated a variety of windowless frozen-hydrogen targets over several years [61, 130]. These target designs rely on the low vapor pressure and good thermal conductivity of solid parahydrogen at $\approx$2–4 K to limit sublimation into the beam vacuum. A recent, successful design for a rare-isotope-beam experiment at TRIUMF is shown in Fig. 23 [130]. As indicated in the figure, the design features a 3–30-μm-thick silver foil stretched over a conical hole in a cooled copper block. To form the target, parahydrogen gas is blown onto the foil through a sintered stainless-steel diffuser and solidifies into a 350-μm-thick film. The diffuser can then be lowered to the "standby" position and the beam turned on; over a 5 mm diameter, the beam sees only hydrogen plus the thin silver foil. During the "hydrogen-blowing" process the beam vacuum in the vicinity of the target is 10^{-7} mbar, improving to 10^{-8} mbar once the hydrogen gas is turned off.

For our experiment, Ishimoto has sketched the new design illustrated in Fig. 24. The cold mass terminates in a notched piece of copper; the notch, shaped as a semicircle-plus-square, can be filled in with solid hydrogen using the retractable diffuser. Retractable front- and back-plates define the target thickness.[14] The 1 mm thickness of the hydrogen is an initial suggestion, but it can be made thinner, perhaps down to 100 μm; an important

[13] With similar considerations, materials in the range Al through Ti were found to be optimal in HERA-B [131].

[14] To prevent the front- and back-plates from sticking to the frozen hydrogen, they are operated at a temperature of $\approx$30 K, somewhat above the freezing point of hydrogen.

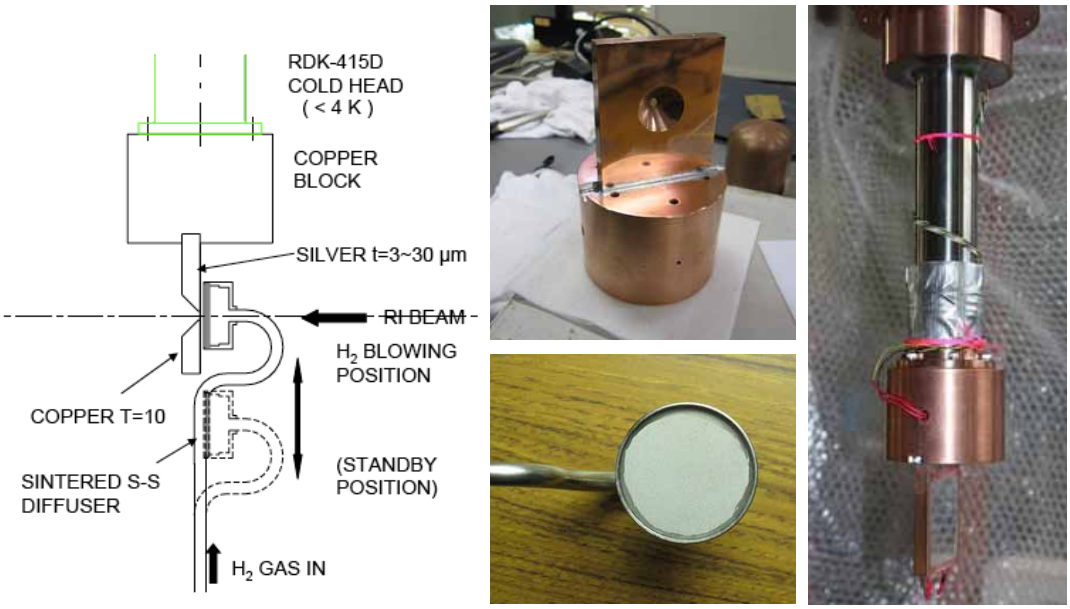

Figure 23: Schematic of solid-hydrogen target built at KEK for TRIUMF experiment, with as-built photos of cold mass, diffuser, and target assembly at right.

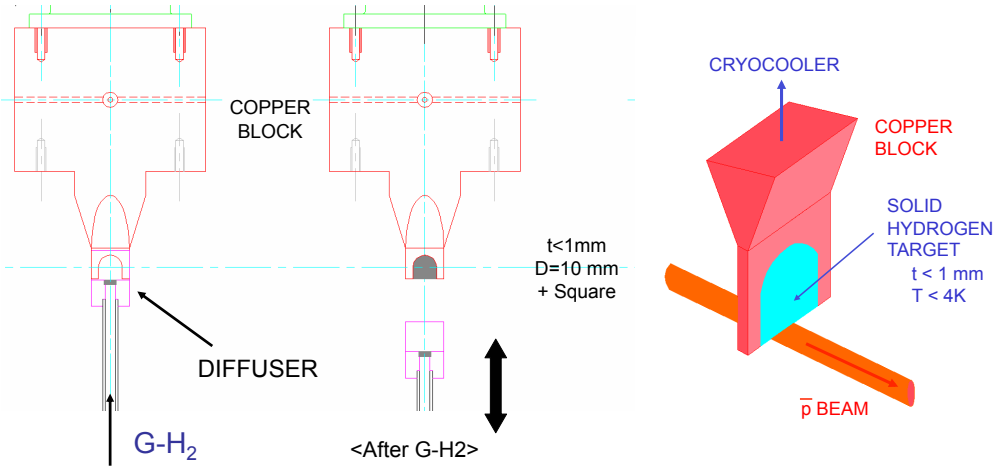

Figure 24: Schematic of solid-hydrogen target proposed for our experiment: left, with diffuser in place over initially empty notch; center, with solid-hydrogen-filled notch (shown in gray), and diffuser retracted; right, 3D schematic of target and beam.

consideration is how wide the notch must be to have a negligible rate of interactions in the copper. Although the 1 cm transverse dimensions of the notch place the copper out of the core of the beam by many standard deviations, some experimentation will be required in order to understand these issues in more detail and determine the practical parameter limits. The design goal is 10^{-7} mbar during hydrogen blowing and 10^{-10} mbar in operation at 2 K.

As an example, we consider a 300 μm thickness of solid hydrogen. The nuclear interaction length of solid hydrogen (SH_2) is $\lambda_I = 591$ cm, thus a 300-μm-thick hydrogen slab

would represent $5.1 \times 10^{-5}\lambda_I$ [19], and a 10 MHz interaction rate will require a rate of antiprotons hitting the target given by

$$R_{\overline{p}} = \frac{R_I}{t} = \frac{10\,\mathrm{MHz}}{5.1 \times 10^{-5}} = 2.0 \times 10^{11}\,\mathrm{Hz}\,. \tag{15}$$

Compared to the circulating antiproton rate, this is (as above) somewhat less than 1 antiproton per million. Approximating the transverse beam distribution in x or y as Gaussian, the target would need to be maintained about 3.5 standard deviations out from the beam center.

The ionization energy-loss rate for antiprotons traversing such a target averages $dE/dx \times t = 0.36\,\mathrm{MeV/cm} \times 0.03\,\mathrm{cm} = 11\,\mathrm{keV}$ per crossing. The radiation length of SH_2 is $X_0 = 716\,\mathrm{cm}$, so the target represents $4.2 \times 10^{-5} X_0$, thus the mean-square multiple-scattering angle of traversing antiprotons is increased at the rate $\approx (14\,\mathrm{MeV}/c\,/\,p)^2\,(x/X_0) = (1.0 \times 10^{-10}\,\mathrm{rad})^2$ per crossing at 8 GeV. These small effects are well within the capability of the stochastic-cooling system.

5.3 Luminosity Monitor

A luminosity monitor will be important in order to achieve small systematic uncertainties in measuring cross sections. A technique that has worked well in many previous experiments (including E760 and E835; see Fig. 1) is to monitor production of particles at right angles to the beam and target. As in past experiments, a small scintillation telescope (possibly with some material interspersed in order to suppress counts from very soft particles) will serve the purpose. Another approach (à la LHC) is also workable: small detectors placed downstream of the experiment at small angles to the beam.

5.4 Magnetic Spectrometer

The final states to be studied feature prominently the charged particles e, μ, π, K, p, and their antiparticles, as well as photons and neutral pions (which decay into photons). The E760 barrel calorimeter [132, 37], with its 1,280 tapered lead-glass blocks all pointing to the antiproton interaction point, has well-established capabilities for identifying and measuring the energies and directions of electrons and photons. However, it produces little information about muons or charged hadrons, whose precise measurement requires the use of a magnetic spectrometer to determine their trajectories and allow reconstruction of their momentum vectors.

A cylindrical geometry offers large solid-angle coverage and thus large acceptance for the produced final states. This consideration motivated the cylindrical layout of the E760 calorimeter (as well as that of the proposed "SuperLEAR" hyperon experiment [57]) and dictates the required geometry of the magnetic spectrometer: a cylindrical, solenoidal magnet that can be inserted into (or, alternatively, surrounding) the E760 calorimeter, with appropriate detectors to precisely measure the trajectories of the charged particles. A similar problem has recently been solved by the Muon Ionization Cooling Experiment (MICE) collaboration [133], who have built (with the participation of the IIT group) solenoidal spectrometers employing thin, planar scintillating-fiber (SciFi) detectors to detect and measure muons of hundred-MeV kinetic energy [134].

Our collaboration includes physicists from CEA Saclay who are interested in providing a small, high-rate time projection chamber (TPC), which could replace the upstream SciFi

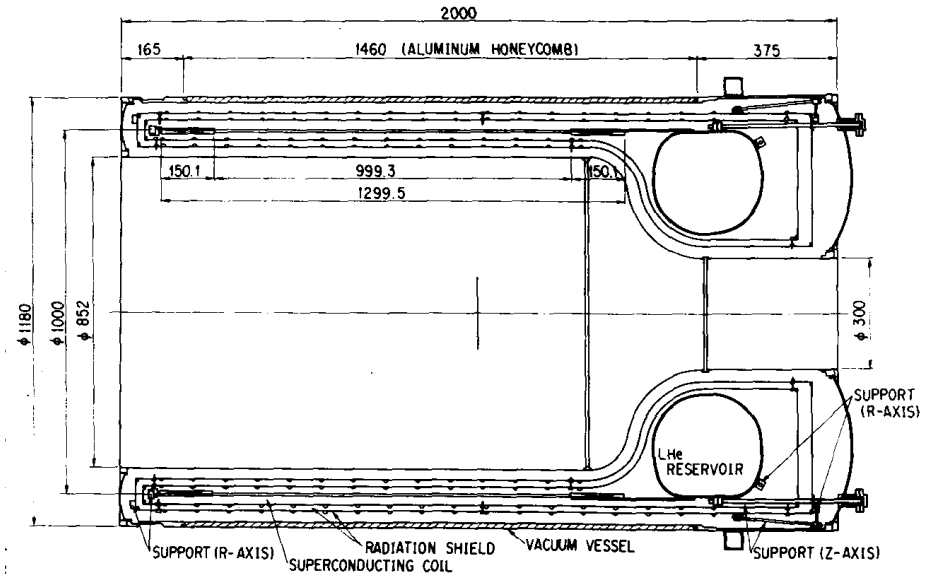

Figure 25: Schematic of BESS solenoid (Ref. [135]); dimensions given in mm.

planes and offer superior tracking performance as well as some particle-ID. Our simulations presented above are based on the SciFi option and show that it is good enough, but at this early stage we make no claim of optimality; optimization will require further studies and may (for example) determine that a configuration with a TPC and fewer SciFi channels suffices, or perhaps is superior, for the physics.[15]

5.4.1 Superconducting solenoid

We have identified a small superconducting solenoid at KEK (Fig. 25), left over from the BESS program of balloon-borne cosmic-ray spectrometers [135], and the KEK Director has graciously given us permission to use it; its properties are summarized in Table 10. The BESS solenoid is wound with aluminum-stabilized superconductor, employs an aluminum-honeycomb cryostat, and thus, at 0.2 radiation lengths, is quite thin (cf. the DØ solenoid at 0.9 radiation lengths [19]), making it almost ideally suited for insertion within a calorimeter. The liquid-helium tank (shown at right in Fig. 25) may need to be removed in order to provide sufficient access to the target area. The BESS solenoid will need to be moved to Fermilab and integrated into the apparatus, and the cryogenics to cool it to LHe temperature will need to be designed, built, and installed. (This system can be shared with that of the VLPCs as discussed below.) Our experience with installation of solenoids and their cryogenics systems for muon cooling R&D indicates that this can conservatively be accomplished within a 2-year period.

5.4.2 Silicon vertex detectors

The Moscow State group has provided silicon detectors for many experiments. Currently they are building detectors for the Compressed Baryonic Matter (CBM) experiment at

[15]Preliminary simulation studies show that minimizing detector material is important to achieving low biases in measuring $\Omega/\overline{\Omega}$ partial-rate asymmetries; in this respect a TPC could thus represent a significant improvement.

Table 10: BESS solenoid parameters.

Parameter	Value	Unit
Outer diameter	1.18	m
Inner bore	0.852	m
Length	2.0	m
Coil diameter	1.0	m
Coil length	1.3	m
Maximum field	1.2	T
Turns	3383	
Nominal current	520	A
Thickness	0.2	rad. length
	0.04	int. length
Superconductor	NbTi/Cu	
Stabilizer	Al (99.999%)	
RRR (Al)	>1000	
Cross section	1.2×1.8	mm^2
Critical current (@3.8 T, 4.2 K)	930	A
LHe capacity	150	liters
Weight	430	kg
Stored energy	815	kJ
Estimated value	1.25	M$

FAIR. These are $4 \times 6\,cm^2$, 250-μm-thick, double-sided detectors with 59 μm pitch and $\pm 7.5^\circ$ stereo angles, and may be suitable for our experiment. These can be configured as wedges and mounted around the beam pipe as shown in Fig. 26. While silicon detectors are not essential to our physics goals, we are discussing the possibility and expect to have more to say about it at a later time. Given the additional multiple Coulomb scattering of silicon as compared to plastic, the detectors and their mounting structures need to be designed with care if the already-good vertex resolution of the SciFi or combined TPC/SciFi system is to be improved upon.

5.4.3 Scintillating-fiber tracking

The MICE spectrometers each employ five planes of scintillating fibers of 350 μm diameter, placed at a pitch of 427 μm in three doublet layers oriented in "60°-stereo" views (Fig. 27), operating within a 4 T solenoid. The MICE fiber thickness is dictated by the need to reduce multiple Coulomb scattering, which dominates their position measurement resolution. Hence, the MICE fibers are ganged by sevens into the readout system, reducing the needed readout channel count correspondingly. The MICE fiber planes are read out using $\approx$8,000 spare channels from the DØ readout system, including the Visible-Light Photon Counter (VLPC) cryogenic photodetectors [136], with their remarkable, >80% quantum efficiency [137, 35]. It is this high quantum efficiency that enables use of the very fine MICE fibers, and of the even-finer fibers we propose. Figure 28 shows the light yield observed in cosmic-ray tests of the MICE trackers, which agrees well with the design value and implies that the fiber diameter can be reduced to 240 μm while maintaining good light yield and reconstruction efficiency.

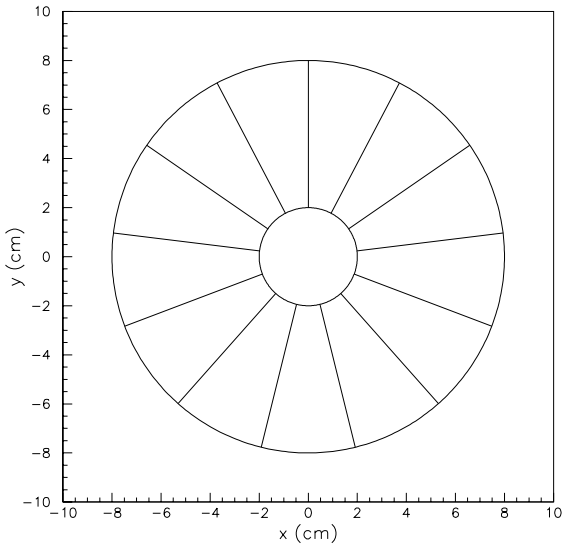

Figure 26: Sketch of possible Silicon Vertex Detector geometry: each disk is composed of 13 sensor wedges with 6 cm radius and 4 cm outer circumference. (Beam pipe fits within inner circle.)

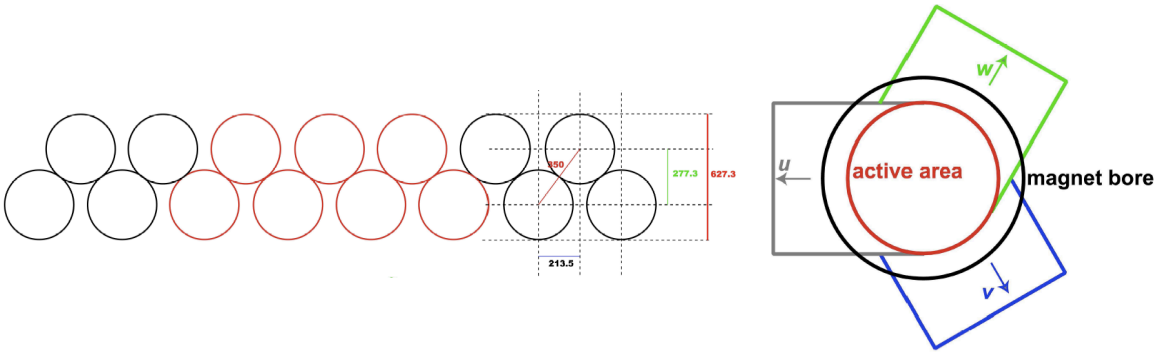

Figure 27: Layout of MICE scintillating-fiber detectors: (left) arrangement of fibers in a doublet; to reduce the needed readout-system channel count, fibers in MICE are ganged for connection to the readout system, with the seven fibers indicated in red connecting to a single VLPC via a 1.05-mm-diameter clear light guide; (right) three doublet layers oriented in 60° stereo.

The proposed antiproton-experiment tracking system will need better position resolution than in MICE, and the higher momenta to be measured in TAPAS reduce the effect of multiple Coulomb scattering. We therefore propose to use 240 μm fibers placed at a pitch of 272 μm, with each fiber individually read out. This yields the channel count of Table 7, requiring the use of most of the DØ readout system (not including those channels already loaned to MICE). Given that the bore of the solenoid (see Section 5.4.1 and Table 10) is slightly smaller than that used in the simulation studies, the channel count of Table 7 will be reduced by ≈10%; with the 20% higher magnetic field, the acceptance will be little affected, and the mass resolution will improve.

The MICE fiber planes are supported within the solenoid bore by a carbon-fiber frame

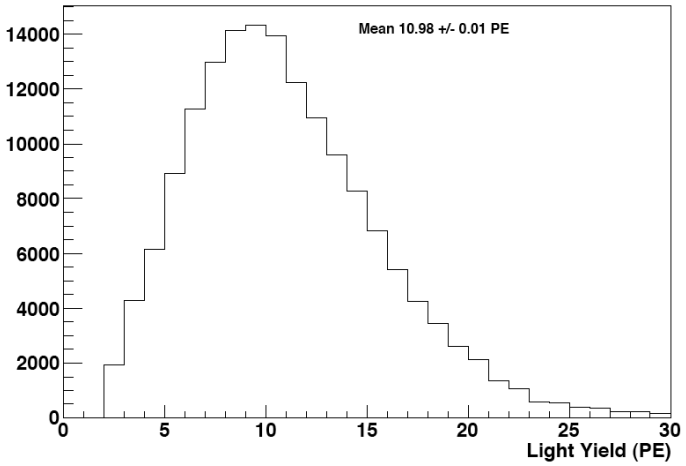

Figure 28: Observed photoelectron yield in MICE tracker cosmic-ray tests.

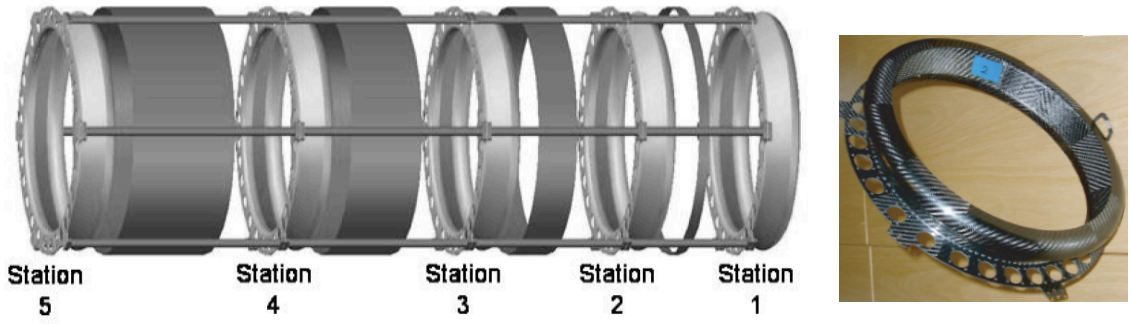

Figure 29: (left) CAD drawing of MICE tracker support frame, showing five carbon-fiber station support bodies mounted on space frame; (right) photo of carbon-fiber station support body.

fabricated by the University of Liverpool group (Fig. 29). We anticipate their contribution in this capacity for the antiproton experiment as well. As indicated in Tables 7 and 10 and Fig. 1, the new planes will cover a larger aperture than the MICE 40 cm bore and will be placed closer together, but the MICE design approach will still serve, and the needed parts will still be within the capabilities of the Liverpool machine shop. The SciFi tracking system built by MICE, comprising some 80,000 fibers, took less than 2 years to assemble and commission. Our estimate of the needed manpower, materials, and cost to build the TAPAS SciFi system (the largest and most complex part of the TAPAS detector effort) is thus reliably based on recent experience.

5.4.4 TPC tracking

Compared with scintillating fibers, a time projection chamber has the advantages of providing many more points per track, along with dE/dx particle-ID information; it also has a significantly smaller channel count and represents less material in the path of the particles. Its disadvantages include coarser position resolution of each measured point (typically $\approx$100–200 μm, compared to 250 μm/$\sqrt{12}$ $\approx$ 70 μm for the SciFi option) and the tens-of-microseconds memory time which, at the $\approx$10 MHz interaction rate at which we propose

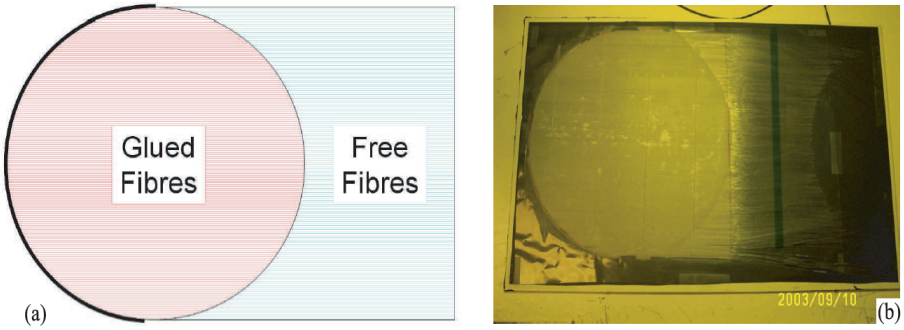

Figure 30: (a) Schematic and (b) photo (taken in yellow light so as not to damage the scintillator) of a MICE scintillating-fiber ribbon as built at Fermilab. Mirrored ends of fibers are to the left. After gluing of ribbons onto station bodies, fiber free ends are glued into optical connectors, trimmed, and polished.

to run, would mean that multiple interactions are typically piled up in each "event." Finally, in contrast to SciFi, which produces fast signals that can be used in the first-level trigger, triggering information using a TPC could be derived only with a complicated online track-finding system. However, this challenge is already being tackled by the $\overline{\mathrm{P}}$ANDA collaboration [138, 139], and we will use similar approaches if we decide to include a TPC in our design.

The challenge for a TPC is the high rates of interactions ($\lesssim 10\,\mathrm{MHz}$) and charged particles ($\lesssim 50\,\mathrm{MHz}$, making some allowance for possible photon conversions in the beam pipe etc.) in $\lesssim 8\,\mathrm{GeV}$ antiproton collisions at $2 \times 10^{32}\,\mathrm{cm}^{-2}\mathrm{s}^{-1}$. While we are unaware of a TPC of the needed dimensions that has been operated at such rates, the KABES detectors for the NA-48/2 experiment constitute reduced-scale prototypes [140]. These feature Micromegas readout, providing sufficient gain with suppressed ion feedback compared to traditional multiwire avalanche detection. They were successfully operated at charged-particle rates up to 70 MHz [140].

5.5 Particle Identification

A time resolution of 10 ps suffices to identify hadrons (Fig. 31) over much of the momentum range of interest, and muons as well, using a detector barrel just outside the solenoid and an endcap disk just inside the downstream end of the solenoid. Such time resolution is already available (but expensive, as discussed in Sec. 6.2) using Cherenkov radiators with commercial microchannel plates (MCPs) and fast time-digitization electronics [141]. We are keeping watch on the Univ. of Chicago "Large-Area Picosecond Photo-Detectors" project, which seeks to develop cost-effective, large-area detector assemblies with performance substantially better than we require [36]. It now appears that such devices will be available on a suitable time-scale (≈ 2013) for initial installation in our experiment. Failing this, we could add them later as an upgrade (the scenario considered in Table 19).

The proposed detector configuration (Fig. 1) includes a TOF barrel and an end-cap covering the downstream solenoid aperture. While the dimensions of the photodetectors will depend on the outcome of the current R&D project, we have sketched one possibility (Fig. 32), based on the geometry of commercially available $4 \times 11\,\mathrm{cm}^2$ Photonis 105X35/12/10/8 MCPs [142]. These are sensitive to within 1 mm of their edges, giving

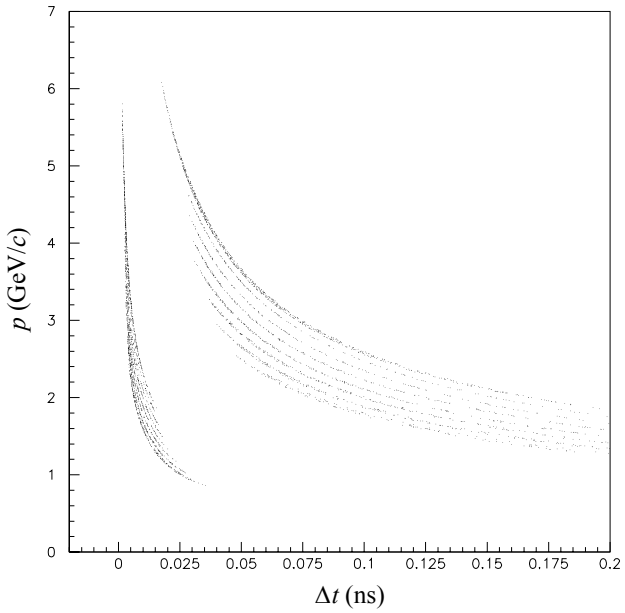

Figure 31: Momentum-vs.-time-difference (Δt) plot for hadrons from simulated D^0 decays accepted by the apparatus; apparent structure is an artifact arising from discrete locations at which time is evaluated in the simulation. With 10 ps Δt resolution, charged kaons (upper-right curves) are separated from charged pions by $>3\sigma$ for $p < 3\,\mathrm{GeV}/c$ and by $>2\sigma$ for $3 < p < 6\,\mathrm{GeV}/c$.

96.6% coverage. The barrel consists of 34 1-cm-thick, 11-cm-wide, 1-m-long quartz radiator plates, each tiled with 25 MCPs, for a total of 850 MCPs; another 114 MCPs can cover the end-cap area. From the viewpoint of multiplicity, coarse segmentation (e.g., one electronics channel per MCP) would suffice. However, since the signal delay depends on location within the MCP, better time resolution will result if each electronics channel corresponds to only a fraction of an MCP. We have budgeted assuming a 3×3 array of electrodes on each MCP, but it's possible that 2×2 would suffice, with attendant cost reduction.

Should the Univ. of Chicago Picosecond project fail to come to fruition in time, another option is to explore the performance of a TOF detector with a substantially reduced number of commercial photodetectors, by relying on the appreciable fraction of Cherenkov light that is totally internally reflected within the quartz radiator plates and thus emerges at their ends, where a reduced number of MCPs will suffice to detect them. If this results in too few photoelectrons, there is room between the 1.18 m solenoid outer diameter and the 1.31 m calorimeter inner bore to increase the thickness of the quartz plates up to about 5 cm. The lengths of the full quartz plates imply up to several nanoseconds in propagation time for internally reflected light, which may make 10 ps resolution difficult. To cope with this, the plates of the barrel could be suitably subdivided into segmented rings read out at their downstream ends. (Hadron identification in this experiment over the needed momentum range can also be partially realized kinematically, as well as, in the TPC tracking option, up to about $1\,\mathrm{GeV}/c$, from ionization data.)

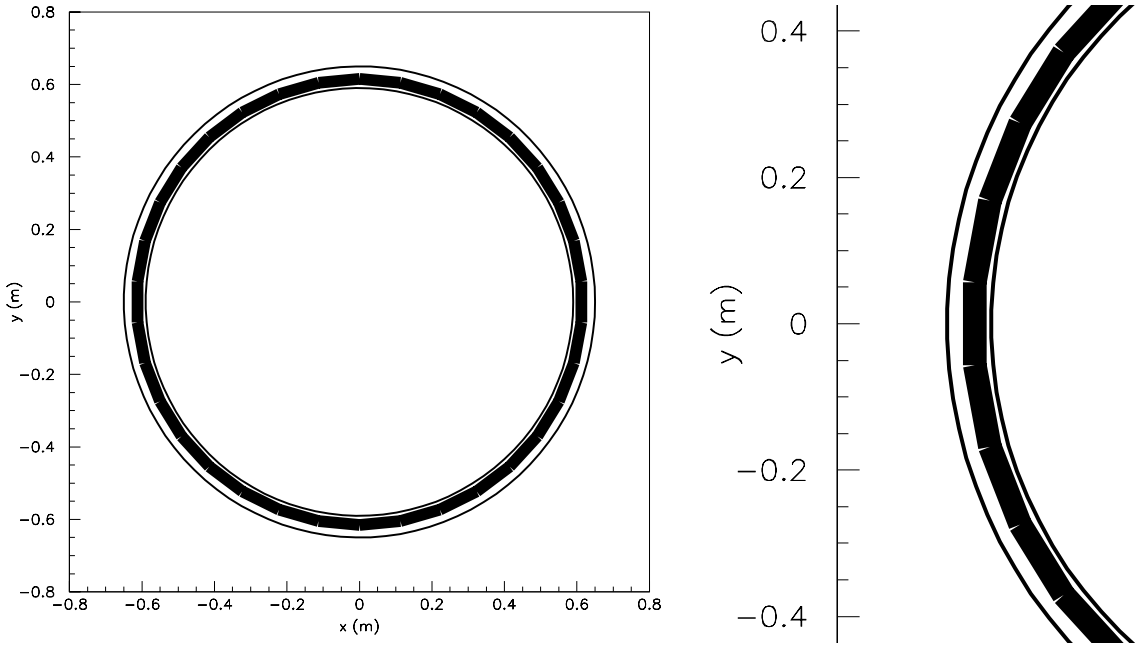

Figure 32: (left) Cross-sectional schematic diagram of TOF Barrel detector, made up of 34 staves (quartz-plate/MCP sandwiches), mounted between solenoid (inner ring) and (outer ring) calorimeter inner bore, together with (right) close-up illustrating individual staves.

5.6 Calorimeter

As already mentioned, the E760 barrel calorimeter [132, 37] consists of 1,280 tapered lead-glass blocks all pointing to the antiproton interaction point, covering polar angles of 10° to 70° with respect to the beam axis. They are arranged in 20 "rings" in polar angle, with each ring subdivided into 64 segments in azimuth; the segmentation in polar angle is visible in Fig. 1. The insertion of the solenoid inside the calorimeter bore should be done in such a way as not to interfere with the performance of the calorimeter photomultiplier tubes (PMTs), requiring that the magnetic field at the PMT locations be $\lesssim 10\,\mathrm{G}$. This will require the use of iron pole faces and a flux return partially enclosing the calorimeter. The forward pole face and flux return will necessarily occlude the five innermost rings of lead-glass blocks, limiting the inner polar-angle coverage to 17.5°. Design and construction of the flux return is a straightforward task that can make use of iron already available at Fermilab.

5.7 Triggers

Level 1 triggering can be done based on hit patterns in the SciFi and TOF counters, as well as energy deposition in the calorimeter. The hit-pattern triggers can be implemented using trigger hardware recycled from DØ [143]. Our goal is to reduce the interaction rate by over an order of magnitude, so that the Level 2 trigger will have to accept no more than about one event per microsecond; if the Level 2 trigger takes of order 1 ms, this will mean fewer than 1,000 events in the Level 2 pipeline on average. With raw events of order 1–10 kB in data length, this requires a buffer of only modest size, hence the Level 2 trigger could actually take considerably more time per event, while still requiring $< 1\,\mathrm{GB}$ of buffer RAM.

While data on $8.9\,\mathrm{GeV}/c$ antiproton reactions are as yet unavailable, Enstrom *et al.* [112]

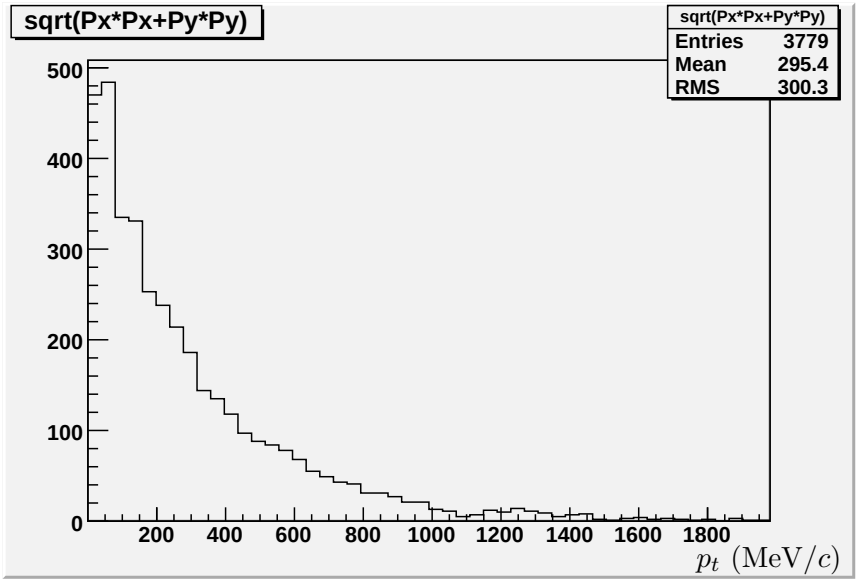

Figure 33: Transverse-momentum histogram of minimum-bias events as generated by Geant4 for 8.9 GeV/c $\overline{p}$-H_2 interactions, as viewed in barrel and end-cap TOF detectors, with a 1 T solenoid field.

have compiled bubble-chamber results on charged-particle multiplicities at 3.66, 5.7, and 6.9 GeV/c. The production cross section for >4 charged tracks is almost constant in this energy range at $\approx(8.2 \pm 1)$ mb. Thus at 2×10^{32} luminosity the rate of such events is ≈ 1.6 MHz. This is an upper limit on the rate at which detector data will need to be digitized and read out, but we can and will do better than this. Typical background events with >4 charged tracks will have tracks with small transverse momenta, thus by doing some additional fast pattern recognition to impose a p_t threshold, we anticipate reducing the rate by another order of magnitude, so that detector digitization and readout can take place at about 100–300 kHz. This is comparable to the event rate in HyperCP [39] and less than the design rate in MICE [144], so is well within the state of the art.

Given the paucity of detailed experimental data, validation of the standard Monte Carlo generators in this energy range is necessarily imperfect, and Monte Carlo predictions of trigger rejection are unlikely to be fully reliable. We have nevertheless used Geant4 [68] to give us some (qualitative, at least) confirmation of the efficacy of this Level 1 approach. Figure 33 shows the transverse-momentum spectrum of minimum-bias events as generated by Geant4 for $\overline{p}$-H_2 interactions at 8.9 GeV/c in our proposed spectrometer. The mean p_t is 295 MeV/c, and 19% of tracks have p_t exceeding 500 MeV/c. Thus requiring that at least one track exceed this p_t threshold will reduce the ≈ 1.6 MHz rate coming out of the multiplicity trigger to $\lesssim 300$ kHz. Figure 15(right) shows that $D^0 \to K\pi$ decays produce very few tracks with transverse momenta below this threshold. If additional rejection is needed at Level 1, a second track can be required to exceed a similar (or possibly, a somewhat reduced) threshold.

We have also used Geant4 to study $\overline{p}$-Ti interactions at 8.9 GeV/c. These have somewhat higher multiplicity and somewhat softer p_t distributions than those in $\overline{p}$-H_2 interactions. The mean p_t according to Geant4 is 240 MeV/c, and 13% of tracks exceed a 500 MeV/c p_t threshold. Thus with nuclear targets the track multiplicity requirement will have somewhat lower, and the track p_t requirement somewhat higher, rejection, but the conclusions above

remain qualitatively unchanged.

Besides the $D^0 \to K\pi$ signal mode considered above, there will also be higher-multiplicity signal events (from, e.g., $D^0 \to K\pi\pi\pi$, $D^0 \to K_S\pi\pi$, $D^+ \to K\pi\pi$, etc.), for which p_t distributions will be softer than those of $D^0 \to K\pi$. High trigger efficiency for such events, with adequate minimum-bias rejection, can be maintained by subjecting higher-multiplicity events to less stringent p_t requirements.

Event pattern recognition (trackfinding) for Level 2 triggering will be performed in a farm of event processing modules, which can make use of detailed tracking and particle-ID detector data. The $\overline{\text{P}}$ANDA collaboration is developing a powerful system for this purpose [138], led by the Univ. of Giessen group, and we are exploring their participation in the Fermilab project (in the years before antiprotons at FAIR become available), or the purchase of "Compute Node" modules of their design. Each Compute Node features five large Xilinx Virtex-4 FPGAs as well as 2 GB of RAM, Gigabit Ethernet, and several high-bandwidth optical links [139]. (It should be noted that our experiment and event complexity will be only a fraction of $\overline{\text{P}}$ANDA's.) Our goal for Level 2 is a further order of magnitude in minimum-bias rejection, which will bring the rate of events to be recorded down to $\approx$10–30 kHz.

Assuming a 100 kHz Level 1 Accept rate, we can estimate the required number of Compute Nodes as follows. To process simulated drift chamber data with 3 tracks per event and 10 hits per track, $\overline{\text{P}}$ANDA found about 60 μs per event for one prototype Compute Node [139]. If our processing time per event were the same, we would need 6 Compute Nodes to keep up with 100 kHz of Level 2 triggers. In these hardware trackfinding algorithms the processing time is typically quadratic in the number of hits and can be made to scale linearly with the number of hits by adding sufficient processing nodes in parallel. Thus to handle the greater hit multiplicity in our events (see Table 11), we would need $4^2 = 16$ times as many modules, or approximately 100 Compute Nodes. We assume further event processing in a 50-node Linux PC farm. (We have budgeted for these systems below, and we note that the estimate corresponds to 15% of that for the BTeV trigger system, which is plausible given the simplicity of our events compared to those in BTeV.) This estimate is arguably conservative in that the scaling of processing time may well go as the square of the number of hits per *plane*, implying a scale factor of $(5/3)^2 \approx 3$ rather than 16, but in planning such systems, our experience shows that it pays to be conservative.

5.8 Data Acquisition System

We take 30 kHz as an upper limit for the rate of events to be recorded. Events will typically be well under 10 kB in length (see Table 11), leading to an upper limit of 300 MB/s, or 6 petabytes/year, comparable to the data rate in CDF or DØ. Given the values in Table 11, more likely, the rate will be less than 3 PB/yr. As a benchmark, HyperCP, with a typical charged multiplicity per triggered event of 2, had 0.5 kB average event size and stored 1×10^5 events/s using 5 VME RAM buffer modules and a large parallel array of Exabyte tape drives [39]. At present the most cost-effective archival storage medium is still magnetic tape (albeit 0.8 TB LTO4 rather than 4 GB Exabyte cartridges), at $\approx$\$45/TB, which may come down by about a factor of 2 within the next year or so when widespread use of Oracle's T10000C drives tapes becomes established [145]. In addition to the cost of tape, current practice at Fermilab is to purchase a 10,000-slot robotic tape-library module for every 10,000 tapes recorded, at an added operating cost of $\approx$0.7 M\$ each [145].

In reading out our SciFi detectors, the DØ scintillating-fiber readout system will need

Table 11: Event length estimate.

Detector	# hits/track	Total # hits	# bytes
SciFi	24	120	480
TOF	1	5	20
Calorimeter	10*	50	200
Subtotal			700
Headers†			70
TOTAL			770

*Based on a calorimeter pulse occupying up to 10 ADC time slices.
†Event and sub-event header words estimated as 10% of total.

to satisfy rather different requirements than in DØ. While the interaction rates are similar (≈10 MHz), the multiplicities and event sizes are quite different, with only about 20 fiber hits expected per event compared to thousands in DØ. However, to cope with their large event size, DØ employs low-level triggers to reduce the frequency of scintillating-fiber readout to about 2 kHz. As discussed above, in the antiproton experiment the low-level trigger will be derived from the fibers themselves, by looking for interesting patterns in the "fast-OR" outputs from the AFE-IIt boards, inconsistent with those of minimum-bias events. We anticipate that this "logic matrix" trigger may be satisfied at a rate of 100 to 300 kHz, thus a faster version of the AFE-IIt microcode will be required. Fortunately, much of this work has already been done for MICE [144], whose design trigger rate is 600 kHz. In the Antiproton Accumulator (unlike the Tevatron Collider and MICE), the beam is debunched, with no radio-frequency time structure, hence the operation of the AFE-IIt boards will need to be synchronized to an arbitrary clock, rather than to the Tevatron crossing time (as in DØ) or (in MICE) the ISIS accelerator clock; however, this can be accomplished with minimal deadtime [143]. As in MICE, we will read out the AFE-IIt system via VLSB modules in several parallel data-streams, using VME systems [146]. The VLPC photodetectors used for the scintillating-fiber tracking detectors operate at a temperature of 9 K; this will require moving a ≈ 600 W helium liquefaction system to the AP-50 experimental area. (The same system will be used to cool the solenoid, whose ∼ 1 W heat load is negligible on this scale; alternatively, if SciFi tracking is not used, the solenoid can be cooled using closed-cycle cryocoolers.)

To enable operation of the E760 calorimeter at luminosities up to $2 \times 10^{32}\,\mathrm{cm}^{-2}\mathrm{s}^{-1}$, as well as to cope with the high anticipated Level 1 trigger rate, we will read out the calorimeter with waveform digitizers of a design recently developed at Fermilab [143, 147].

6 Budget and Schedule

6.1 Summary of Recuperated Equipment

Our proposed experiment design is based on the availability of substantial amounts of very capable equipment and material:

- The E760 barrel calorimeter is in storage at Fermilab.
- The BESS spectrometer solenoid is available at KEK.

- The old CDF and DØ beryllium beam pipes are in storage at Fermilab.
- The 100,000-channel DØ scintillating-fiber readout system (VLPCs, VLPC cryostats, and AFE-IIt cards) is available now that the Tevatron program has ended.
- The DØ and CDF Level 1 trigger systems are also available.
- Large numbers of VME crates, with their power supplies, master computers, and other interfaces, are also available from CDF and DØ.
- High-quality iron for the magnet yoke is available at Fermilab.

6.2 Budget Summary

Table 3 gives an overall budget summary. Tables 12 to 18 summarize our budget estimates by subsystem. We note that much of the total budget should be obtainable in university research grants from NSF and DOE (both the Nuclear Physics and Elementary Particle/High Energy Physics programs). The high-bandwidth data-acquisition and Level 2 triggering farm we propose is well suited to $\overline{\mathrm{P}}$ANDA as well as to TAPAS and (given the likely schedule for antiprotons at FAIR) could conceivably be used by each experiment in succession; alternatively, the system developed for our experiment could be inexpensively replicated for $\overline{\mathrm{P}}$ANDA, since, given Moore's Law, the software and firmware development cost for such systems is likely to outweigh the hardware cost for replication in ≈ 2016.

Budget estimates for targets are given in Table 12, including the frozen-hydrogen target and assuming that we build three wire targets of three different materials.

A budget estimate for the Luminosity Monitor is given in Table 13.

We present in Table 14 the estimated cost for building the proposed 80,000-channel scintillating-fiber tracking system. We are less knowledgeable as to the cost of building and instrumenting a high-rate TPC, but are confident that it would be significantly less than that of the SciFi option; fundamentally, many fewer parts need to be handled in order to assemble a TPC, whereas for a SciFi system, every individual fiber must be manually laid in place, threaded through connectors, and read out by VLPCs maintained at a temperature of 9 K.

Concerning the TOF budget, the Large-Area Picosecond Photodetector project leadership is reluctant to project future costs, but the goal is that they be substantially less than that of current devices. In view of this, we present here an approximate estimate based on existing commercial technology (Table 15), with the proviso that we do not plan to seek funds for this level of expenditure. If the cost of the new devices is not established in time for the current round of budgeting, we could defer this detector and install it later as an upgrade (the assumption underlying Table 19).

A Trigger budget estimate is given in Table 16. It assumes reuse of very capable trigger systems from Tevatron experiments.

Data acquisition will be done largely via VME, using crates and interfaces recuperated from CDF and DØ. The calorimeter signals will be digitized via flash-ADC modules of a recent Fermilab design [147]. Since some of the lead-glass blocks will be obscured by the forward part of the return yoke, only 960 of the 1,280 channels will need to be instrumented. We have included funds for spares.

The largest item of infrastructure is the cryogenics system. It and other anticipated infrastructure costs are summarized in Table 18. Much of this will consist of existing equipment and materials (cryogenics equipment, return-yoke iron, beam pipe) at Fermilab.

Table 12: Target Budget Estimate.

Type	Cost (k$)	Cont'cy (k$)	Basis
Wire	30	10	
Solid hydrogen	400	150	S. Ishimoto, KEK
TOTALS	430	160	

Table 13: Luminosity Monitor Budget Estimate.

Item	Cost (k$)	Cont'cy (k$)	Basis
Scintillation telescope	50	15	
Electronics	10	5	
TOTALS	60	20	

Table 14: SciFi Budget Estimate.

Type	Number	Cost (k$)	Cont'cy (k$)	Basis
Scintillating fiber	90 km	40	20	Kuraray (MICE quote)
Clear fiber	300 km	280	140	Kuraray (MICE quote)
Engineering effort	2 FTE-yr	500	150	MICE
Technician effort	6 FTE-yr	600	200	MICE
Fiber mirroring		100	25	MICE
Optical connectors		200	50	MICE
Support structure		100	25	MICE
TOTALS		1,820	610	

Table 15: Time-of-Flight Budget Estimate.*

Type	Number	Unit cost (k$)	Cost (k$)	Cont'cy (k$)	Basis
MCP	1,000	7	7,000	3,000	Photonis, Inc.
Quartz plates	40	2.5	100	30	SPI
Electronics	10,000	0.25	2,500	500	CAEN
VME systems†	13				
TOTALS*			9,600*	3,530*	

*Note that we do not plan to use this commercial solution; we present its budget here for illustrative purposes only (see discussion in text).
†Available from CDF and DØ.

Table 16: Trigger Systems Budget Estimate.

Item	Number	Unit cost (k$)	Cost (k$)	Cont'cy (k$)	Basis
Level 1*					P. Rubinov, FNAL
L2 Compute Nodes	100	9	900	300	P. Rubinov, FNAL
L2 Farm nodes	50	2	100	30	
Postdoc effort	3 FTE-yr		270	90	
Student effort	3 FTE-yr		120	40	
TOTALS			1,390	460	

*Level 1 trigger from DØ.

Table 17: Data Acquisition Budget Estimate.

Item	Number	Unit cost (k$)	Cost (k$)	Cont'cy (k$)	Basis
Calorimeter flash ADC	1,200	0.10	120	30	P. Rubinov, FNAL
VME system*	TBD	0	0	0	
Data buffering system	1		10	3	M. Crawford, FNAL
Tape drive+host node	5	18	90	30	M. Crawford, FNAL
Postdoc effort	2 FTE-yr		180	60	
Student effort	2 FTE-yr		90	30	
TOTALS			490	153	

*Available from CDF and DØ.

Table 18: Infrastructure Budget Estimate.

Item	Cost (k$)	Cont'cy (k$)	Basis
Assemble and install solenoid flux return	300	100	Vl. Kashikhin, FNAL
Cryogenics & solenoid installation	900	400	M. Green, LBNL, R. Rucinski, FNAL
Install Be beam pipe	50	20	
Install cables	100	30	
TOTALS	1,350	550	

6.3 Schedule

With the Tevatron run now over, the opportunity to build and install the needed equipment is upon us, limited primarily by experiment approval and funding. In a "technologically limited" schedule, we could aim to begin commissioning when accelerator operations resume in 2013. Given the inevitable delay from approval to availability of grant funds, such a schedule is likely too tight, and commissioning in 2014 is a more-likely-achievable goal. We present in Table 19 an illustrative guesstimated schedule, which of course will need to be refined in the light of what we actually find in running the experiment.

Table 19: Illustrative Schedule Estimate: after about two years of assembly and installation, apparatus shakedown and data-taking will take about four years.

Activity	Duration (mo)
Apparatus shakedown & debugging	6
Find $X(3872)$ and measure cross section	1
Measure $\sigma(D^*)$ and $\sigma(D)$	1
Measure $\sigma(\overline{\Omega}\Omega)$	1
Study/scan charmonium states	1
Dedicated $X(3872)$ run	12*
Dedicated hyperon CPV run	12*
Install & debug particle-ID (TOF) upgrade	3*
Charm CPV/Drell–Yan run	12*

*Durations of precision physics runs depend on cross sections, to be measured in early running. Latter part of schedule will likely be revised based on what is learned in former part.

7 Collaboration

We view the author list of this proposal as only a subset of the eventual collaboration. While it is arguably already sufficiently strong to carry out the technical work needed, we are in discussion with several additional physicists from a number of institutions who have expressed strong interest but have not yet decided to join our collaboration. With approval of the proposal and funding of the work, many individual investigators already in the collaboration will be joined by postdocs and students, and additional physicists and institutions will join as well.

8 Competition for the Facility

It has been proposed that the $g-2$ experiment be moved from Brookhaven to Fermilab and installed near the Antiproton Source, with the antiproton production target and Debuncher ring used to produce the needed muon beam. The proposed modification of the Debuncher can be done in such a way as to maintain compatibility with antiproton operation [148]. Since we need to use the Debuncher only ≈ 10 to 15% of the time, and $g-2$ propose to run only part of the time, this represents only a minor impact on $g-2$.

Use of the Antiproton Source has also been discussed for the Mu2e experiment. As far as we know, this cannot be done in such a way as to maintain compatibility with antiproton running, but it is not out of the question that a compatible solution could be found. Absent a compatible solution, we are committed to making way for Mu2e when the time comes; we are confident that this will leave a sufficient window for the success of TAPAS.

On the other hand, recent discussion of using the Recycler to produce the Mu2e proton beam [149] suggests that availability of the Antiproton Source for antiproton physics could continue for many more years, well into the "FAIR era." Since our program focuses on just a few topics requiring the highest luminosities, where Fermilab holds the advantage over FAIR, and theirs exploits the greater flexibility of FAIR and the $\overline{\mathrm{P}}$ANDA detector for a wide range of Nuclear Physics studies, the simultaneous operation of both facilities would be a sensible scenario.

The Antiproton Source is a unique facility in the world. Its value for antiproton physics is substantial and should not be dismissed without careful evaluation and consideration. Having optimized this unique capability at great effort and expense in order to do the best Tevatron Collider physics possible, we have a responsibility to exploit it as thoroughly as possible after the end of the Tevatron program.

References

* We are grateful to M. Vagins for suggesting this acronym.

[1] See `http://www.gsi.de/fair/index_e.html`

[2] E. Eichten, K. Lane, and C. Quigg, Phys. Rev. D **73**, 014014 (2006); Erratum-*ibid.* **73**, 079903 (2006).

[3] See e.g. Sec. 3.9 of M. Artuso, G. Buchalla, *et al.*, *Report of Working Group 2 of the CERN Workshop "Flavour in the era of the LHC,"* Geneva, Switzerland, November 2005 – March 2007, Eur. Phys. J. C **57**, 309–492 (2008).

[4] V. M. Abazov *et al.* [DØ Collaboration], "Evidence for an anomalous like-sign dimuon charge asymmetry," Phys. Rev. Lett. **105**, 081801 (2010).

[5] See e.g. I. I. Bigi and N. Uraltsev, Nucl. Phys. B **592** (2001) 92.

[6] A. D. Sakharov, Pisma Zh. Eksp. Teor. Fiz. **5**, 32 (1967) [Sov. Phys. JETP Lett. **5**, 24 (1967)].

[7] H. Quinn, Nucl. Phys. Proc. Suppl. **50** (1996) 17;
A. G. Cohen, D. B. Kaplan, A. E. Nelson, Ann. Rev. Nucl. Part. Sci. **43**, 27 (1993);
P. Huet and E. Sather, Phys. Rev. D **51**, 379 (1995).

[8] See e.g. X.-G. He, H. Murayama, S. Pakvasa, and G. Valencia, Phys. Rev. D **61**, 071701R (1999).

[9] See e.g. L. Hall and S. Weinberg, Phys. Rev. D **48**, R979 (1993).

[10] A. Le Yaouanc, L. Oliver, and J.-C. Raynal, Phys. Lett. B **292** (1992) 353.

[11] M. Gronau and S. Wakaizumi, Phys. Rev. Lett. **68**, 1814 (1992);
A. Le Yaouanc *et al.*, LPTHE-Orsay/95-15, hep-ph/9504270 (1995).

[12] V. A. Kostelecký, Phys. Rev. D **69**, 105009 (2004).

[13] G. Perez, presented at *PANIC11: The 19th Particles and Nuclei Int. Conf.*, MIT, Cambridge, MA, July 24–29, 2011, `http://web.mit.edu/panic11/talks/tuesday/PLENARY-2P/2-905/perez/980-0-GiPerezPlenary.pdf`.

[14] E. Golowich, J. Hewett, S. Pakvasa and A. A. Petrov, Phys. Rev. D **76**, 095009 (2007).

[15] See e.g. A. A. Petrov, arXiv:0806.2498 [hep-ph], and references therein.

[16] M. Artuso, B. Meadows and A. A. Petrov, Ann. Rev. Nucl. Part. Sci. **58**, 249 (2008).

[17] C. Materniak, presented at *Eighth Int. Conf. on Hyperons, Charm and Beauty Hadrons (BEACH08)*, Columbia, SC, 22–28 June 2008, Nucl. Phys. Proc. Suppl. **187** (2009) 208;
C. Materniak *et al.* [HyperCP Collaboration], in preparation.

[18] H. K. Park *et al.* [HyperCP Collaboration], Phys. Rev. Lett. **94**, 021801 (2005).

[19] K. Nakamura *et al.* [Particle Data Group], J. Phys. G **37**, 075021 (2010).

[20] S. K. Choi *et al.* [Belle Collaboration], Phys. Rev. Lett. **91**, 262001 (2003).

[21] B. Aubert *et al.* [BABAR Collaboration], Phys. Rev. D **71**, 071103 (2005).

[22] D. Acosta *et al.* [CDF-II Collaboration], Phys. Rev. Lett. **93**, 072001 (2004).

[23] V. M. Abazov *et al.* [DØ Collaboration], Phys. Rev. Lett. **93**, 162002 (2004).

[24] K. Abe *et al.* [Belle Collaboration], arXiv:hep-ex/0408116.

[25] K. Abe *et al.* [Belle Collaboration], "Evidence for $X(3872) \to \gamma J/\psi$ and the sub-threshold decay $X(3872) \to \omega J/\psi$," arXiv:hep-ex/0505037.

[26] G. Gokhroo *et al.* [Belle Collaboration], Phys. Rev. Lett. **97**, 162002 (2006).

[27] B. Aubert *et al.* [BABAR Collaboration], Phys. Rev. Lett. **102**, 132001 (2009).

[28] B. Aubert *et al.* [BABAR Collaboration], Phys. Rev. D **77**, 011102R (2008).

[29] T. A. Armstrong *et al.* [E760 Collaboration], Phys. Rev. D **47**, 772 (1993).

[30] M. Andreotti *et al.* [E835 Collaboration], Phys. Lett. B **654** (2007) 74.

[31] N. Brambilla *et al.* [Quarkonium Working Group], *Heavy Quarkonium Physics*, CERN Yellow Report CERN-2005-005 (2005);
N. Brambilla *et al.* [Quarkonium Working Group], "Heavy quarkonium: progress, puzzles, and opportunities," Eur. Phys. J. **C71** (2011) 1534.

[32] I. I. Bigi, "No Pain, No Gain – On the Challenges and Promises of Charm Studies," presented at Charm09, Leimen, Germany, May 2009, available at `https://indico.gsi.de/getFile.py/access?contribId=45&sessionId=14&resId=0&materialId=0&confId=442`, arXiv:0907.2950 [hep-ph].

[33] C. A. Chavez, "D^0-$\overline{D}^0$ Mixing at BABAR," in *Proc. 2009 Europhysics Conference on High Energy Physics*, July 16–22, 2009, Krakow, Poland, e-Print PoS (EPS-HEP 2009) 187.

[34] Fermilab P-986 letter of intent and addenda:
`http://www.fnal.gov/directorate/program_planning/Mar2009PACPublic/P986LOIFeb2009.pdf`;
`http://capp.iit.edu/hep/pbar/P-986-Addendum.pdf`;
`http://capp.iit.edu/hep/pbar/P-986-Addendum2.pdf`;
see also `http://capp.iit.edu/hep/pbar/`.

[35] V. M. Abazov *et al.* [DØ Collaboration], Nucl. Instrum. Meth. A **565** (2006) 463.

[36] H. Frisch, Univ. of Chicago, private communication;
see `http://psec.uchicago.edu/`.

[37] G. Garzoglio *et al.* [E835 Collaboration], Nucl. Instrum. Meth. A **519** (2004) 558.

[38] M. Kotulla *et al.* [$\overline{\text{P}}$ANDA Collaboration], Technical Progress Report for: $\overline{\text{P}}$ANDA, available from `http://www-panda.gsi.de/auto/doc/pap/papers.htm`.

[39] R. A. Burnstein *et al.* [HyperCP Collaboration], Nucl. Instrum. Meth. A **541** (2005) 516.

[40] J. F. Donoghue, X.-G. He, S. Pakvasa, Phys. Rev. D **34**, 833 (1986);
X.-G. He, H. Steger, G. Valencia, Phys. Lett. B **272** (1991) 411.

[41] T. D. Lee and C. N. Yang, Phys. Rev. **108**, 1645 (1957).

[42] L. C. Lu *et al.* [HyperCP Collaboration], Phys. Rev. Lett. **96**, 242001 (2006).

[43] J. Tandean, Phys. Rev. D **70**, 076005 (2004);
J. Tandean and G. Valencia, Phys. Lett. B **451** (1999) 382.

[44] O. Kamaev *et al.* [HyperCP Collaboration], "Study of the rare hyperon decay $\Omega^{\mp} \to \Xi^{\mp}\pi^{+}\pi^{-}$," Phys. Lett. B **693** (2010) 236.

[45] X.-G. He, J. Tandean, G. Valencia, Phys. Lett. B **631** (2005) 100;
N. G. Deshpande, G. Eilam, J. Jiang, Phys. Lett. B **632** (2006) 212.

[46] D. S. Gorbunov, V. A. Rubakov, Phys. Rev. D **64**, 054008 (2001);
D. S. Gorbunov, Nucl. Phys. B **602** (2001) 213;
X.-G. He, J. Tandean, G. Valencia, Phys. Lett. B **631** (2005) 100.

[47] J. D. Bjorken, private communication.

[48] M. Reece and L.-T. Wang, JHEP07 (2009) 051;
M. Pospelov, Phys. Rev. D **80**, 095002 (2009);
C.-H. Chen, C.-Q. Geng, and C.-W. Kao, Phys. Lett. B **663** (2008) 400.

[49] L. Bellantoni (for the KTeV Collaboration), "Search for $K_L \to \pi^0\pi^0\mu^+\mu^-$ with KTeV Data," arXiv:0911.4516 [hep-ex] (2009);
Y. C. Tung *et al.* [E391a Collaboration], Phys. Rev. Lett. **102**, 051802 (2009);
A. V. Artamonov *et al.* [BNL-E949 Collaboration], Phys. Rev. D **79**, 092004 (2009).

[50] H. J. Hyun *et al.* [Belle Collaboration], Phys. Rev. Lett. **105**, 091801 (2010);
V. M. Abazov *et al.* [DØ Collaboration], Phys. Rev. Lett. **103**, 061801 (2009);
W. Love *et al.* [CLEO Collaboration], Phys. Rev. Lett. **101**, 151802 (2008);
B. Aubert *et al.* [BABAR Collaboration], Phys. Rev. Lett. **103**, 081803 (2009).

[51] S. Oh, J. Tandean, JHEP01 (2010) 022;
X.-G. He, private communication;
J. Tandean, private communication.

[52] T. Johansson, in *Proc. Eighth Int. Conf. on Low Energy Antiproton Physics (LEAP '05)*, Bonn, Germany, 16–22 May 2005, AIP Conf. Proc. **796**, 95 (2005).

[53] C. Y. Chien *et al.*, Phys. Rev. **152**, 1181 (1966).

[54] C. Baltay *et al.*, Phys. Rev. **140**, B1027 (1965).

[55] Markward Britsch, "Hyperon Production in Proton–Nucleus Collisions at 42-GeV Center of Mass Energy," diploma thesis, Max-Planck-Institute for Nuclear Physics, Heidelberg (2003).

[56] High-Energy Reactions Analysis Group, report CERN-HERA-84-01 (1984).

[57] N. Hamann *et al.* [CP-Hyperon Study Group], report CERN/SPSLC 92019, SPSLC/M491, 30 March 1992.

[58] E. Braaten and J. Stapleton, Phys. Rev. D **81**, 014019 (2010).

[59] D. P. McGinnis, G. Stancari, S. J. Werkema, Nucl. Instrum. Meth. A **506** (2003) 205.

[60] N. A. Tørnqvist, Phys. Lett. B **590** (2004) 209.

[61] See e.g. S. Ishimoto *et al.*, Nucl. Instrum. Meth. A **480** (2002) 304.

[62] E. Braaten, Phys. Rev. D **73**, 011501R (2006).

[63] E. Braaten, Phys. Rev. D **77**, 034019 (2008).

[64] T. A. Armstrong *et al.* [E760 Collaboration], Nucl. Phys. B **373** (1992) 35.

[65] B. Aubert *et al.* [BABAR Collaboration], Phys. Rev. Lett. **96**, 052002 (2006).

[66] See `http://belle.kek.jp/superb/`.

[67] P. Reimer, private communication. (Based on a CTEQ code.)

[68] We used the G4beamline "wrapper" for Geant4, with the FRITIOF hadronization and Bertini cascade models (as recommended for accurate modeling of hadron calorimetry below 10 GeV); see `http://www.muonsinc.com/tiki-index.php?page=G4beamline` (we also verified that using other Geant4 physics models made only minor differences).

[69] C. S. Lam and W. K. Tung, Phys. Rev. D **21**, 2712 (1980).

[70] S. Falciano *et al.* [NA10 Collaboration], Z. Phys. **C31**, 513 (1986).

[71] J. S. Conway *et al.* [E615 Collaboration], Phys. Rev. D **39**, 92 (1989).

[72] L. Y. Zhu *et al.* [E866 Collaboration], Phys. Rev. Lett. **99**, 082301 (2007).

[73] L. Y. Zhu *et al.* [E866 Collaboration], Phys. Rev. Lett. **102**, 182001 (2009).

[74] T. Aaltonen *et al.* [CDF Collaboration], Phys. Rev. Lett. **106**, 241801 (2011).

[75] D. Boer, Phys. Rev. D **60**, 014012 (1999).

[76] J. Erler and M. Ramsey-Musolf, Phys. Rev. D **72**, 073003 (2005).

[77] W. Hwang, G. Garvey, J. Moss, and J.C. Peng, Phys. Rev. D **39**, 209 (1989).

[78] H. Shimizu *et al.*, Phys. Rev. D **71**, 114007 (2005).

[79] Heavy-Flavor Averaging Group, `http://www.slac.stanford.edu/xorg/hfag/charm/`.

[80] See e.g. M. E. Mattson, "Precision measurements of CP violation and D0-D0bar mixing at CDF," presented at 35th Int. Conf. on High Energy Physics, Paris, France, July 22–28, 2010, available at `http://indico.cern.ch/contributionDisplay.py?contribId=1082&confId=73513`.

[81] See e.g. Y. Grossman, A. L. Kagan, Y. Nir, Phys. Rev. D **75**, 036008 (2007).

[82] M. Kotulla *et al.* [$\overline{\mathrm{P}}$ANDA Collaboration], Letter of Intent (2004).

[83] E. Eichten and C. Quigg, private communication.

[84] Using Eq. 5 of Ref. [63], we obtain 1.3 μb.

[85] A. I. Titov and B. Kämpfer, Phys. Rev. C **78**, 025201 (2008).

[86] A. Titov, private communication.

[87] M. J. Leitch *et al.*, Phys. Rev. Lett. **72**, 2542 (1994).

[88] C. Lourenço, H. K. Wöhri, Phys. Rep. **433** (2006) 127–180.

[89] B. Aubert *et al.* [BABAR Collaboration], Phys. Rev. Lett. **98**, 211802 (2007).

[90] M. Starič *et al.* [Belle Collaboration], Phys. Rev. Lett. **98**, 211803 (2007).

[91] T. Aaltonen it et al. [CDF Collaboration], Phys. Rev. Lett. **100**, 121802 (2008).

[92] B. Aubert *et al.* [BABAR Collaboration], Phys. Rev. D **78**, 011105 (2008).

[93] L. M. Zhang *et al.* [Belle Collaboration], Phys. Rev. Lett. **99**, 131803 (2007).

[94] B. Aubert *et al.* [BABAR Collaboration], Phys. Rev. D **78**, 034023 (2008);
P. del Amo Sanchez *et al.* [BABAR Collaboration], Phys. Rev. Lett. **105**, 081803 (2010).

[95] D. M. Asner *et al.* [CLEO Collaboration], Phys. Rev. D **72**, 012001 (2005).

[96] Y. Nir, Lectures given at *27th SLAC Summer Institute on Particle Physics: CP Violation in and Beyond the Standard Model (SSI 99)*, Stanford, CA, 7–16 July 1999, in **Particle Physics** (Trieste, 1999), pp. 165–243;
S. Bergmann *et al.*, Phys. Lett. B **486**, 418 (2000).

[97] D. M. Asner *et al.* [CLEO Collaboration], Phys. Rev. D **70**, 091101R (2004).

[98] See e.g. I. I. Bigi, "The Expected, the Promised and the Conceivable – On *CP* Violation in Beauty and Charm Decays," in Frascati Phys. Ser. **3** (1994) 235.

[99] S. Pakvasa, "Charm as Probe of New Physics," in *The Future of High-Sensitivity Charm Experiments (Proc. Charm2000 Workshop)*," ed. D. M. Kaplan and S. Kwan, FERMILAB-Conf-94/190 (1994), p. 85.

[100] Z. Xing, Phys. Lett. B **353** (1995) 313.

[101] J. M. Link *et al.* [FOCUS Collaboration], Phys. Lett. B **618** (2005) 23.

[102] L. M. Zhang *et al.* [BELLE Collaboration], Phys. Rev. Lett. **96**, 151801 (2006).

[103] A. A. Petrov, "CP-violation in charm," presented at *6th Int. Workshop on the CKM Unitarity Triangle (CKM2010)*, Univ. of Warwick, UK, 6–10 Sept. 2010, arXiv:1101.3822 [hep-ph].

[104] M. Petrič *et al.* [BELLE Collaboration], Phys. Rev. D **81**, 091102 (2010).

[105] R. Harr (for the CDF Collaboration), presented at *34th Int. Conf. on High Energy Physics (ICHEP08)*, Philadelphia, 2008, arXiv:0810.3444 [hep-ex].

[106] C. Amsler *et al.*, Phys. Lett. B **639** (2006) 165.

[107] S. N. Ganguli *et al.*, Nucl. Phys. B **183** (1981) 295.

[108] E. Braaten, private communication.

[109] A. D. Frawley, T. Ullrich, R. Vogt, Phys Rep. **462** (2008) 125–175.

[110] A. Aleev *et al.* [SVD-2 Collaboration], arXiv:1004.3676 [hep-ex].

[111] See `http://ppd.fnal.gov/experiments/e907/`; we are grateful to the MIPP collaboration for making these data available to us.

[112] J. E. Enstrom, T. Ferbel, P. F. Slattery, B. L. Werner [Particle Data Group], Report LBL-58, May 1972.

[113] M. Gaździcki and D. Röhrich, Z. Phys. C **71**, 55 (1996).

[114] L. Maiani, F. Piccinini, A. D. Polosa, V. Riquer, Phys. Rev. D **71**, 014028 (2005).

[115] O. Piskunova, in preparation.

[116] A. I. Veselov, O. I. Piskunova, K. A. Ter-Martirosian, Phys. Lett. B **158** (1985) 175.

[117] M. I. Adamovich *et al.* [WA89 Collaboration], Eur. Phys. J. C **26** (2003) 357.

[118] D. Drijard *et al.*, Z. Phys. C **12** (1982) 217.

[119] B. I. Abelev *et al.* [STAR Collaboration], Phys. Rev. C **75**, 064901 (2007).

[120] G. Bocquet *et al.* [UA1 Collaboration], Phys. Lett. B **366** (1996) 441.

[121] D. Acosta *et al.* [CDF-II Collaboration], Phys. Rev. D **72**, 052001 (2005).

[122] H. J. Lipkin, "Frontiers of the Quark Model," in *Proc. Les Houches Workshop 1987.*

[123] R. L. Jaffe, Phys. Rev. Lett. **38**, 195 (1977).

[124] See (among many others):
A. Martinez Torres, E. Oset, Phys. Rev. Lett. **105**, 092001 (2010) and Phys. Rev. C **81**, 055202 (2010);
K. Ghoroku, A. Nakamura, T. Taminato, F. Toyoda, JHEP08 (2010) 007;
D. Diakonov, "Prediction of new charmed and bottom exotic pentaquarks," arXiv:1003.2157 [hep-ph];
M. Karliner, H. J. Lipkin, "About a Possible Nonstrange Cousin of the Θ^+ Pentaquark," arXiv:1002.4149 [hep-ph];
P. Gubler *et al.*, Nucl. Phys. A **835** (2010) 342;
N. A. Baltzell, PhD thesis, Univ. of S. Carolina (2009).

[125] E. M. Aitala *et al.*, Phys. Rev. Lett. **81**, 44 (1998).

[126] H. Nakayama, "Status and Plans for SuperKEKB and Belle II experiment," Feb. 24, 2011.

[127] G. Wilkinson, "News from the flavour frontier – heavy quark physics at the LHC," talk presented at The 2011 Europhysics Conference on High Energy Physics (EPS 2011), Grenoble, France, `http://eps-hep2011.eu/`.

[128] S. D. Drell and T.-M. Yan, Phys. Rev. Lett. **25**, 316 (1970); Ann. Phys. **66**, 578 (1971).

[129] H. Orth, GSI-Darmstadt, private communication.

[130] S. Ishimoto *et al.*, "Thin Windowless Solid Hydrogen Target," RCNP-Prog-Report-426, Research Center for Nuclear Physics, Osaka Univ.

[131] K. Ehret, Nucl. Instrum. Meth. A **446** (2000) 190.

[132] L. Bartoszek *et al.* [E760 Collaboration], Nucl. Instrum. Meth. A **301** (1991) 47.

[133] MICE Collaboration: see `http://mice.it.edu/` and, e.g., F. J. P. Soler, "Status of MICE," in *Proc. NuFact09 Workshop*, ed. D. M. Kaplan, M. Goodman, Z. Sullivan, AIP Conf. Proc. **1222**, 288 (2010).

[134] M. Ellis *et al.*, "The design, construction, and performance of the MICE scintillating fibre trackers," Nucl. Instrum. Meth. A **659** (2011) 136; arXiv:1005.3491 [physics.ins-det].

[135] Y. Makida *et al.*, Adv. Cryo. Eng. **37A**, 167 (1992);
Y. Makida *et al.*, IEEE Trans. Appl. Supercond. **5**, 174 (1995).

[136] M. Petroff and M. Stapelbroek, "Photon-Counting Solid-State Photomultiplier," IEEE Trans Nucl. Sci. **36**, 158 (1989);
M. Petroff and M. Atac, "High-Energy Particle Tracking using Scintillation Fibers and Solid-State Photomultipliers," IEEE Trans Nucl. Sci. **36**, 163 (1989).

[137] A. Bross *et al.*, Nucl. Instrum. Meth. A **477** (2002) 172.

[138] W. Korcyl *et al.*, IEEE Trans. Nucl. Sci. **55**, 429 (2008).

[139] M. Liu, "ATCA-Based Computation Platform for Data Acquisition and Triggering in Particle Physics Experiments," *Proc. Int. Conf. on Field Programmable Logic and Applications*, Heidelberg (2008), p. 287.

[140] B. Peyaud, Nucl. Instrum. Meth. A **535** (2004) 247.

[141] J. Va'vra *et al.*, Nucl. Instrum. Meth. A **606** (2009) 404.

[142] Photonis Corp., private communication.

[143] P. Rubinov, Fermilab, private communication.

[144] T. Hart, *MICE Tracker Data Acquisition Using DØ Analog Front End IIt Boards*, MICE Note 139 (2006), available at `http://mice.iit.edu/micenotes/public/doc/MICE0139/MICE0139.doc`.

[145] M. Crawford, Fermilab, private communication.

[146] T. Hart, *VME LVDS SerDes Buffer (VLSB) Boards for MICE Tracker Readout*, MICE Note 178 (2007), available at http://mice.iit.edu/micenotes/public/doc/MICE0178/MICE0178.doc.

[147] P. Rubinov, talk presented at Fermilab All Experimenters Meeting, March 22, 2010, http://www.fnal.gov/directorate/program_planning/all_experimenters_meetings/special_reports/Rubinov_T995_03_22_10.pptx.

[148] S. Nagaitsev, private communication.

[149] M. Popovic, "Concept: Mu2e with Slow Spill from the Recycler," Beams-doc-3974-v2 (2011), http://beamdocs.fnal.gov/AD-public/DocDB/ShowDocument?docid=3974.